NATIONAL ADVISORY COMMITTEE FOR AERONAUTICS

WARTIME REPORT

ORIGINALLY ISSUED
April 1944 as
Advance Restricted Report L4D03

WIND-TUNNEL INVESTIGATION OF CONTROL-SURFACE CHARACTERISTICS

XVI - PRESSURE DISTRIBUTION OVER AN NACA 0009 AIRFOIL WITH 0.30-AIRFOIL-CHORD BEVELED-TRAILING-EDGE FLAPS

By H. Page Hoggard, Jr., and Marjorie E. Bulloch

Langley Memorial Aeronautical Laboratory
Langley Field, Va.

WASHINGTON

NATIONAL ADVISORY COMMITTEE FOR AERONAUTICS

ADVANCE RESTRICTED REPORT NO. L4D03

WIND-TUNNEL INVESTIGATION OF CONTROL-SURFACE CHARACTERISTICS XVI - PRESSURE DISTRIBUTION OVER AN NACA 0009 AIRFOIL WITH 0.30-AIRFOIL-CHORD BEVELED-TRAILING-EDGE FLAPS

By H. Page Hoggard, Jr., and Marjorie E. Bulloch

SUMMARY

Pressure-distribution tests have been made in the NACA 4- by 6-foot vertical tunnel of a plain flap with interchangeable beveled trailing edges on an NACA 0009 airfoil. The flap chord was 30 percent of the airfoil chord and the bevel chords were 15 and 20 percent of the flap chord. The 15-percent bevel was tested with the bevel corner faired with both large and small radii. The purpose of these tests was to supply pressure-distribution data that may be used for structural and aerodynamic design of horizontal and vertical tail surfaces.

The results are presented as diagrams of resultant pressure coefficients and of increments of resultant pressure coefficient for the airfoil with the flap having beveled trailing edges. The diagrams are presented for the control surface with the gap at the flap nose sealed and unsealed.

A comparison of the beveled-flap pressure data with plain-flap data indicated that the addition of a bevel reduced the pressures over the entire airfoil, including the peak at the airfoil nose, and caused a reversal of pressure over the beveled part of the flap. The normal-force coefficient for the beveled-trailing-edge flap was less than the coefficient for the plain-airfoil-contour flap. The open gap produced a tendency toward overbalance by decreasing the negative pressures over the upper surface of a flap when deflected downward. The results generally were in fair agreement with force-test data previously published.

INTRODUCTION

The National Advisory Committee for Aeronautics has instituted an extensive investigation of the aerodynamic characteristics of various control surfaces. The force-test data from this investigation have been summarized in reference 1. The two-dimensional pressure-distribution data obtained as part of the investigation have been analyzed and the variation with flap chord of the various aerodynamic characteristics of a flap has been presented in reference 2.

Two-dimensional force tests have been previously run on a similar model of an NACA 0009 airfoil with several beveled trailing edges; the results of these tests are presented in reference 3 (also summarized in reference 1). From the results of these force tests of trailing-edge shapes having various included trailing-edge angles and other airfoil tests, a method based on the included angle at the trailing edge has been found for predicting the values of hinge-moment parameters to be expected from a bevel. This correlation can be found in figure 150 of reference 1.

The two-dimensional-flow tests presented herein were made to investigate the pressure acting on a control surface with a beveled trailing edge. Such data should be valuable for structural design of the control surfaces, for explanation of the balancing action of the bevel, and for study of boundary-layer conditions. The investigation was made at all angles of attack and flap deflections considered necessary for the structural design of ailerons, elevators, and rudders.

SYMBOLS

c_f	flap chord rearward of flap hinge axis, percent airfoil chord
c	chord of basic airfoil with flap neutral
q	dynamic pressure of free air stream
P	pressure coefficient

P_R resultant pressure coefficient

ΔP_R increment of resultant pressure coefficient

p static pressure at a point on airfoil

p_o static pressure in free air stream

α_o angle of attack for infinite aspect ratio

δ_f flap deflection

M Mach number, ratio of local velocity to speed of sound

c_n airfoil section normal-force coefficient (n/qc)

c_m airfoil section pitching-moment coefficient about quarter-chord point of airfoil (m/qc^2)

c_{n_f} flap section normal-force coefficient (n_f/qc_f)

c_{h_f} flap section hinge-moment coefficient (h_f/qc_f^2)

n normal force of airfoil section per unit span

m pitching moment of airfoil section about quarter-chord point per unit span

n_f normal force of flap section per unit span

h_f hinge moment of flap section per unit span

$$c_{n_\alpha} = \left(\frac{\partial c_n}{\partial \alpha_o}\right)_{\delta_f}$$

$$c_{n_{\alpha_{free}}} = \left(\frac{\partial c_n}{\partial \alpha_o}\right)_{c_{h_f}=0}$$

$$\alpha_\delta = \left(\frac{\partial \alpha_o}{\partial \delta_f}\right)_{c_n}$$

$$c_{n_{f_\alpha}} = \left(\frac{\partial c_{n_f}}{\partial \alpha_o}\right)_{\delta_f}$$

$$c_{n_{f_\delta}} = \left(\frac{\partial c_{n_f}}{\partial \delta_f}\right)_{\alpha_o}$$

$$c_{h_{f_\alpha}} = \left(\frac{\partial c_{h_f}}{\partial \alpha_o}\right)_{\delta_f}$$

$$c_{h_{f_\delta}} = \left(\frac{\partial c_{h_f}}{\partial \delta_f}\right)_{\alpha_o}$$

$$P_\alpha = \left(\frac{\partial P}{\partial \alpha_o}\right)_{\delta_f}$$

$$P_\delta = \left(\frac{\partial P}{\partial \delta_f}\right)_{\alpha_o}$$

The subscripts outside the parentheses indicate the factors held constant during the measurement of the parameter.

Subscripts:

U point on upper surface

L point on lower surface

R resultant

APPARATUS AND MODELS

The tests were made in the NACA 4- by 6-foot vertical tunnel. The test section of this tunnel has been converted from the original open, circular, 5-foot-diameter jet (reference 4) to a closed rectangular 4- by 6-foot test section, as shown in figure 1. The model completely spanned the test section; therefore, two-dimensional flow was approximated.

The model used for the pressure-distribution tests of this investigation was designed to be an exact copy of the model used for the force tests in reference 3 but with only the $0.15c_f$ and $0.20c_f$ beveled-trailing-edge shapes. The $0.15c_f$ bevel was tested with the bevel corner faired with both large and small radii. The 2-foot-chord model was made of laminated mahogany to the modified NACA 0009 profile (table I). The airfoil was equipped with a 0.30c plain flap, as shown in figure 2(a). A gap of 0.005c was provided at the flap nose. The flap was constructed with interchangeable blocks that formed a beveled trailing edge and a thickened profile, as shown in figure 3 of reference 3.

A single chordwise row of pressure orifices was built into the upper and lower surfaces of the airfoil and flap at the midspan location. The orifice locations are presented in figure 2(b) in percent of airfoil chord from the leading edge. The copper tubes from the pressure orifices were brought out of the model at one end through the torque tube and the tunnel wall to a multiple-tube, open-faced manometer. Readings were recorded by a camera.

TESTS

All of the tests, except those with large flap deflection and high positive angle of attack (flap deflection, 30° and 45°; angle of attack, 14.3° and 19.3°) were run at an average dynamic pressure of 15 pounds per square foot. The large flap deflections at high positive angles of attack required more power than was available to maintain a dynamic pressure of 15 pounds per square foot; therefore, these tests were run at an average dynamic pressure of 12 pounds per square foot. The airspeed in the test section at dynamic pressures of 15 and 12 pounds per square foot is about 76 and 69 miles per hour, respectively, at standard sea-level conditions. The corresponding values of effective Reynolds number are 2,760,000 and 2,208,000. (Effective Reynolds number = Test Reynolds number × Turbulence factor; the turbulence factor of the NACA 4- by 6-foot vertical tunnel is 1.93.)

The tests were made at angles of attack ranging from -20° to 20° at intervals of 5° and at angles giving maximum positive and negative lift. It may be noted that all

angles of attack are offset from the exact values of 0°, 5°, 10°, 15°, and 20° by -0.7° owing to an error in setting the zero angle of attack. This error was found to be consistent throughout the tests and the data were corrected accordingly. The model was tested with the 0.30c plain flap deflected 0°, 1°, 2°, 5°, 10°, 15°, 20°, 25°, 30°, and 45°. The tests were run with the flap gap both open (0.005c gap) and sealed with plasticine. During the tests with 30° and 45° flap deflection, pressure orifice 15 for the lower surface (fig. 2(b)) was sealed because its position at both large flap deflections was inside the gap.

Check tests were made for each flap deflection as an indication of the accuracy of the test results. When the 0.005c gap was used, the check tests were made after both angle of attack and flap deflection had been reset. The sealed-gap check tests had only the angle of attack reset, because the plasticine seal would have to be refaired if the flap deflection were changed.

The speed of the tunnel was maintained at the test value of q for approximately 2 minutes before readings were recorded in order to allow the alcohol in the manometer tubes to reach the correct height.

RESULTS

Presentation of Data

The results of the pressure-distribution tests are given in the form of diagrams of resultant pressures with flap neutral and resultant-pressure increments caused by varying the flap deflection. The resultant pressures and increments of resultant pressure are presented for the various bevel and gap combinations and for various angles of attack in figures 3 to 10. The resultant normal pressure at any point along the chord of the airfoil was determined by taking the algebraic difference of the pressures normal to the upper and lower surfaces of the airfoil at that point. All diagrams of resultant pressures or resultant-pressure increments of the airfoil and flap combinations are plotted as pressure coefficient P_R or as ΔP_R. The resultant pressure coefficient is defined as

$$P_R = P_L - P_U$$

where

$$P_U = \frac{p_U - p_o}{q}$$

$$P_L = \frac{p_L - p_o}{q}$$

P pressure coefficient

p static pressure at a point on airfoil

p_o static pressure in free air stream

q dynamic pressure of free air stream

and the subscripts

U upper surface

L lower surface

R resultant

The resultant-pressure diagram for any condition may be obtained by adding the distribution at a given angle of attack and the distribution at a given flap deflection. A comparison of resultant-pressure distributions over the bevel juncture with large and small radii is presented in figure 11 at several angles of attack and flap deflections.

Pressure distributions for the upper and lower surfaces of the flap having a $0.15c_f$ bevel with sealed gap are presented in figure 12 for various angles of attack and flap deflections. The resultant pressures over the NACA 0009 airfoil with 0.30c plain flap and sealed gap (reference 5) are compared with the resultant pressures over the modified airfoil with $0.15c_f$-bevel flap in figure 13. Figure 14 presents upper- and lower-surface pressures over the plain flap and the $0.15c_f$-bevel flap for the same conditions for which resultant pressures are given in figure 13.

The rates of change of pressure coefficient with angle of attack and with flap deflection are presented for

the various bevel and gap combinations in figures 15 to 18 for convenience in calculating distributions at small values of α_o and δ_f. The flap section normal-force coefficient as a function of flap deflection is presented for all combinations of bevel and gap in figures 19 and 20 at several angles of attack. Complete chordwise pressure distributions for various combinations of α_o and δ_f that might occur on the horizontal tail of a dive bomber in highly accelerated maneuvers at various speeds are presented in figure 21 for the $0.15c_f$-bevel flap with sealed gap.

The section aerodynamic coefficients of the airfoil and flap are presented as functions of angle of attack for all bevel and gap combinations in figures 22 to 24. The coefficients were obtained in each case by mechanical integration of the original pressure diagrams.

The parameter values for beveled flaps are presented in table II along with values for the plain-airfoil-contour flap for convenient comparison. The plain-flap parameter values were obtained from references 1 and 6.

Precision

The angles of attack are believed accurate within $\pm 0.1^\circ$. Flap deflections are believed accurate within $\pm 0.2^\circ$. Plotted values of pressure coefficient P are correct within ± 2 percent except for peaks at the leading edge and flap hinge axis or for stalled conditions.

Coefficient values calculated from check test points have been plotted in figures 19 and 22 and are designated by flagged symbols. Many of the points come within the accuracy of the plot; others vary a negligible amount. The accuracy of the corrected zero angle of attack is indicated by the deviation from zero of lift and moment coefficients at zero angle of attack. From figures 19 and 22, it appears that the maximum error in setting the angle of attack at zero lift is 0.2°. This discrepancy may be caused by flow misalinement in the tunnel or by an asymmetrical model.

Two-dimensional flow having been approximated, the results may be considered as section characteristics.

Experimental tunnel corrections were applied only to the airfoil section normal-force coefficient c_n. Although no corrections were made for the other coefficients, the tunnel values are believed to be higher than the free-air values and hence are on the conservative side for structural purposes. The magnitude of the airfoil resultant pressure coefficients as represented in the resultant-pressure diagrams (figs. 3 to 10) is known to be too large by about 7 percent because these curves were plotted directly from manometer records without the application of the experimental tunnel correction, which allows for the increase in lift produced by tunnel-wall interference.

DISCUSSION

Resultant-Pressure Distribution

The resultant-pressure diagrams should prove useful in determining loading conditions for the structural design of ailerons and horizontal and vertical control surfaces. Tests have indicated that the increments of pressure and the increments of section aerodynamic coefficients caused by flap deflection are approximately independent of the airfoil section for airfoils of approximately the same maximum thickness and thickness distribution (references 7 and 8). It is therefore believed that, for structural design, the incremental data presented herein may be applied to other basic sections of approximately the same thickness and thickness distribution. The increments of the section aerodynamic coefficients may be taken from figures 22 to 24 by using the flap-neutral curve as a reference line.

From a study of the incremental-resultant-pressure curves for the stalled conditions ($\alpha_o = 19.3^\circ$ and -20.7°) for both bevel chords and gap conditions (figs. 4, 6, 8, and 10), it appears that the bevel continues to reduce the flap hinge moment in the stalled condition from the hinge moment for a plain flap under the same conditions. The tests of beveled elevators on the fuselage of a typical pursuit airplane also indicated that the bevel was effective in the stalled attitude and reduced the floating angle of the elevators by about 10° (reference 9) from the angle at which airfoil-contour elevators would float. The resultant-pressure curves (figs. 3 to 10), especially for the 0.005c gap, show a tendency toward a decrease of resultant pressure over the main airfoil just ahead of the flap.

The results indicate that the size of the radius at the bevel juncture is relatively unimportant in its effect on the loads over a beveled-trailing-edge flap (fig. 11).

Pressure Distribution over Upper and Lower Surfaces of Beveled Flap

The distributions presented at various angles of attack and flap deflections in figure 12 indicate that only on the surface of the flap which is deflected against the relative wind does the bevel affect the pressure distribution to any great extent. The only exceptions occur at low angles of attack and small flap deflections, for which the upper- and lower-surface distributions show nearly equal effect of bevel. The pressure distribution on the side away from the relative wind, when at large angles of attack or flap deflection, resembles that of a flap and tab in a stalled condition.

It will be noticed in figure 13 that the resultant-pressure peak at the flap hinge axis is higher for the beveled flap with the 0.005c gap than for the beveled flap with the sealed gap. Inasmuch as the resultant pressure is the algebraic difference of the upper- and lower-surface pressures at any point, the positive peak on the lower surface makes the resultant-pressure peak higher. (See fig. 14.)

The pressure distribution produced over the upper and lower surfaces of a flap by a beveled trailing edge is compared with the pressures over a plain flap in figure 14. The effect on the pressure distribution of the bevel on the surface deflected against the relative wind is more pronounced when the gap is open. The main effect of the open gap on the flap pressure distribution appears to be the decrease in magnitude of the negative pressures over the upper surface of the flap, which results in a tendency toward lower or even overbalanced hinge moments.

Curves of P_α and P_δ

For convenience in calculating the pressure distributions over both surfaces for small values of α_o

and δ_f, the curves of P_α and P_δ were calculated and are presented in figures 15 to 18. From the experimental data, it was found impossible to predict with any degree of accuracy the variation of pressure with angle of attack over the nose of the airfoil because the stagnation point moves considerably and the pressures change rapidly and are not linear with angle of attack. The variation of pressure with angle of attack over the rest of the airfoil appeared from these tests to remain a linear variation only from 0° to 5°; therefore, the P_α-curves should not be used for calculating pressures beyond a value of α_o of 5°.

The variation of pressure with flap deflection for any point on the airfoil contour appeared from these tests to be linear to 5°. The P_δ-curves therefore should not be used for flap deflections greater than 5°. The final pressure distribution required is found by multiplying the values of P_α and P_δ by the values of α_o and δ_f for which the distribution is desired and adding algebraically to the basic distribution (P at $\alpha_o = \delta_f = 0°$) given in the lower part of figures 15 to 18.

Flap Section Normal-Force Coefficient

For all combinations of bevel and gap tested, the values of c_{n_f} were smaller than for the plain flap with sealed gap at the same angles of attack. The values of $c_{n_{f_\alpha}}$ and $c_{n_{f_\delta}}$ for beveled and plain flap may be conveniently compared in table II. The variation of c_{n_f} as a function of angle of attack is clearly shown in figures 19 and 20. The effect of α is small at $\delta_f = 28°$ with the gap open and at $\delta_f = 20°$ with the gap sealed.

Pressure Distribution on Horizontal Tail For Highly Accelerated Maneuvers

The flight condition during which high structural loads and the formation of a compression shock on the horizontal tail are most likely to occur is a highly

accelerated maneuver in which the horizontal tail is operating at a high angle of attack at high speed. The pressure data presented herein are not applicable to tail design for high-speed flight unless they are corrected for the variation of pressure with Mach number, which is given approximately by the relation $1/\sqrt{1 - M^2}$. Theoretical variations of pressure with Mach number are compared with experimental pressure-distribution data at various Mach numbers in reference 10. The pressure distributions presented in figure 21 at angles of attack of -0.7°, 5.7°, and 10.7° and with flap deflections of 0°, -5°, -10°, and -15° are test data that cover the highly accelerated maneuvers estimated from unpublished dive-bomber test data.

Aerodynamic Section Characteristics

Normal-force coefficient.- The force-test lift data of reference 3 are given in terms of section lift coefficient whereas the pressure-distribution data are given in terms of normal-force coefficient. Inasmuch as the lift coefficient and normal-force coefficient have nearly the same value, this value is referred to as "lift" in the following discussion.

The slope of the lift curve $\left(\frac{\partial c_n}{\partial \alpha_o}\right)_{\delta_f}$ from table II for the airfoil with $0.15c_f$ beveled trailing edge and sealed gap is 0.088 as compared with 0.091 from the force-test data in reference 3. These results are in fair agreement if account is taken of the fact that different models and methods of calculation were used for the force and pressure tests.

The lift-curve slopes from the force and pressure tests for the $0.20c_f$ bevel with sealed gap have the same value, 0.092. For the open gap the lift-curve slopes from the force and pressure tests are, respectively, 0.088 and 0.087 (table II and reference 1). The lift-curve slopes obtained from the pressure-distribution tests appear to check very well with the force-test results. Opening the gap appeared to change the angle of attack at which the stall occurred by about 1°. This angle of attack, approximately ±12° with flap neutral, was not affected by bevel chord.

The values of lift effectiveness $\left(\frac{\partial \alpha_o}{\partial \delta_f}\right)_{c_n}$ given in table II were taken at zero lift and show the expected decrease in effectiveness as a result of the beveled trailing edge. The small radius on the bevel juncture increased c_{n_α} about 0.003 for open and sealed gap when compared with the lift-curve slope for the large-radius bevel. Reducing the radius at the bevel juncture decreased the effectiveness from -0.56 to -0.52.

The parameter $c_{n_{\alpha_{free}}}$ (table II) is a measure of control-free stability only at $\alpha_o = \delta_f = 0°$. The values in table II indicate the expected tendency of the beveled flap to float upward at a smaller angle than the plain flap.

A method for estimating the pressure distribution (and normal force) over a bevel from available tab pressure-distribution data is given in the appendix. The results of this method are illustrated and a comparison is made in figure 25, at several angles of attack and flap deflections, between actual and estimated pressure distributions for a $0.20c_f$ bevel with sealed gap and an included angle at the trailing edge of 25°.

Flap hinge-moment coefficient.- The values of $c_{h_{f_\alpha}}$ (table II) were taken over the linear part of the hinge-moment curve, which was over a small range (±5°) for the 0.005c-gap tests and a larger range (±10°) for the sealed-gap tests (figs. 22 and 24). The values of $c_{h_{f_\delta}}$ (table II) were taken from $\delta_f = 0°$ to $\delta_f = 5°$ because the curve appeared linear over this range. For a complete picture of the effect of various bevel and gap combinations, all the hinge-moment curves (figs. 22 to 24) must be taken into consideration and too much reliance should not be placed on the slope values measured over a small part of each curve, except for stick-free stability calculations.

The values of $c_{h_{f_\alpha}}$ and $c_{h_{f_\delta}}$ as found for the $0.15c_f$ and $0.20c_f$ bevels with sealed gap are in fair agreement with the values of reference 3. Values of both hinge-moment parameters for the 0.20c bevel with 0.005c gap

were read from the curves in figure 49 of reference 1 and were found to be in fairly close agreement. The values of $c_{h_{f_\alpha}}$ and $c_{h_{f_\delta}}$ for both bevel chords were found to fall near the correlation curve of figure 150 in reference 1 with less scatter than the average scatter of the correlation points.

From the values of hinge-moment parameters in table II it appears that decreasing the radius at the bevel juncture tends to decrease the negative values of $c_{h_{f_\delta}}$ for both gap conditions. Decreasing the radius had no effect on the value of $c_{h_{f_\alpha}}$ when the gap was open but decreased the positive value when the gap was sealed.

Pitching-moment coefficient.- The slopes of the curves of pitching-moment coefficient as a function of lift coefficient at a constant angle of attack and at a constant flap deflection are given in table II. The aerodynamic center of additional lift caused by varying the angle of attack generally was located at approximately the 0.22c station for the sealed-gap tests and the 0.21c station for the 0.005c-gap tests. The bevel chord had little effect on the location of this aerodynamic center.

The aerodynamic center at which the lift produced by flap deflection may be considered to act is located at approximately the 0.41c station for either gap condition. All aerodynamic-center locations for the gap-sealed condition are in fair agreement with the values presented in reference 3.

CONCLUSIONS

Pressure-distribution tests have been made in the NACA 4- by 6-foot vertical tunnel of a plain flap with interchangeable beveled trailing edges on an NACA 0009 airfoil. The flap chord was 30 percent of the airfoil chord and the bevel chords were 15 and 20 percent of the flap chord. The results of these tests indicated the following conclusions:

1. At a given angle of attack and flap deflection, the addition of a bevel reduced the resultant pressures over the entire airfoil, except for the pressure at the flap hinge axis, including the peak at the airfoil nose, and caused a reversal of pressure over the beveled part of the flap.

2. The normal-force coefficient for the beveled-trailing-edge flap was less than the coefficient for the plain-airfoil-contour flap with the airfoil at the same angle of attack and the flap deflected through the same angle.

3. The open gap at the flap nose gave the flap a tendency toward overbalance because of a decrease in the negative pressures over the upper surface of a downward deflected beveled flap and because of a slight increase in the negative peak on the lower-surface bevel juncture.

4. The size of the radius used to fair the bevel juncture appeared to have no appreciable effect on the pressure distribution developed.

5. The results obtained from the pressure-distribution tests generally were in fair agreement with force-test results of a comparable arrangement.

Langley Memorial Aeronautical Laboratory,
National Advisory Committee for Aeronautics,
Langley Field, Va.

APPENDIX

METHOD FOR CALCULATING PRESSURE DISTRIBUTION OVER A BEVEL FROM TAB PRESSURE-DISTRIBUTION DATA

When an elevator, aileron, or rudder is designed, the general practice is to use the total load over the surface. Motion pictures of bulged fabric on ailerons in high-speed dives indicate that the pressures along the chord should be used to determine how securely the covering must be fastened to the structural members. In the case of a beveled surface for which a pressure peak occurs at the bevel juncture, a study of the chordwise distribution might prevent a covering failure. A method for predicting the chordwise pressure distribution over a beveled surface without having to test it is advantageous, particularly as such a method supplements a method already established for predicting the hinge-moment characteristics.

A method for predicting the chordwise load distribution on the flap is described herein. No attempt is made to predict flap section hinge-moment coefficients; the hinge-moment correlation based on the included angle at the trailing edge (for sealed-gap condition) may be found in figure 150 of reference 1.

The bevel contour was developed (fig. 3 of reference 3) by deflecting a $0.20c_f$ tab $\pm 10^\circ$ and deflecting the flap slightly each way to keep the tab trailing edge centered on the airfoil chord line. Inasmuch as the bevel profile was developed by using deflected-tab contours, it was decided to use tab pressure diagrams to estimate the pressure distribution of a beveled flap. Only the upper-surface distribution for a tab deflected downward and the lower-surface distribution for a tab deflected upward are considered. It is necessary to correct these pressures by means of P_δ to allow for the small flap deflections necessary to keep the tab trailing edge centered on the airfoil chord line. The resulting diagrams (fig. 25) were integrated and found to give values of c_{n_f} that were in good agreement with the bevel test data for flap deflections of 10° and 20° at values of α_o of -0.7° and 4.3° (figs. 25(c), 25(d), 25(g), and 25(h)). The value of c_{n_f} based on tab

data was in general somewhat larger than the bevel test value.

At the smaller flap deflections, the values of c_{n_f} from tab data were generally much larger than from bevel test data but, from a comparison of the values with those for a plain flap in figure 20, the estimated values were found to be closer to the bevel test values than to the plain-flap values.

In order to use the present correlation method, it is necessary to have pressure-distribution diagrams for a flap and tab of the desired chords. The tab chord should approximately equal the distance from bevel juncture to trailing edge.

The included angle of the bevel must be reproduced by the correct tab and flap deflections. These deflections must be found in order that the tab-deflection diagram may be chosen and corrected. The following equation gives the amount that the flap must be deflected to keep the tab trailing edge centered on the airfoil chord line:

$$\Delta\delta_f = \sin^{-1} \frac{c_t \sin \frac{\phi_{bevel} - \phi_{airfoil}}{2}}{c_f - c_t}$$

where

ϕ_{bevel} included angle at trailing edge of bevel (for which prediction is being made)

$\phi_{airfoil}$ included angle at trailing edge of airfoil from tests of which flap and tab pressure diagrams are to be used

c_t chord of tab, percent airfoil chord

c_f chord of flap, percent airfoil chord

With $\Delta\delta_f$, ϕ_{bevel}, and $\phi_{airfoil}$ known the angle through which the tab is deflected $\pm\delta_t$ to reproduce the included angle of the bevel may be found by the following equation:

$$\pm\delta_t = \Delta\delta_f + \frac{\phi_{bevel} - \phi_{airfoil}}{2} \qquad (1)$$

It may be noticed in figure 25 that the tab data used were for $\delta_t = \pm 10^\circ$ whereas equation (1) gives $\delta_t = \pm 8.40^\circ$. By using the diagrams for $\delta_t = \pm 10^\circ$, the included angle was found to be 27.6° instead of the correct value of 25°; but, inasmuch as the correlation for the hinge-moment parameters based on included angle shows a change of 0.001 in the value of the hinge-moment parameters for a change of 2° in the included angle, there could be only a slight change in the size or shape of the pressure diagram.

REFERENCES

1. Sears, Richard I.: Wind-Tunnel Data on the Aerodynamic Characteristics of Airplane Control Surfaces. NACA ACR No. 3L08, 1943.

2. Ames, Milton B., Jr., and Sears, Richard I.: Determination of Control-Surface Characteristics from NACA Plain-Flap and Tab Data. NACA Rep. No. 721, 1941.

3. Jones, Robert T., and Ames, Milton B., Jr.: Wind-Tunnel Investigation of Control-Surface Characteristics. V - The Use of a Beveled Trailing Edge to Reduce the Hinge Moment of a Control Surface. NACA ARR, March 1942.

4. Wenzinger, Carl J., and Harris, Thomas A.: The Vertical Wind Tunnel of the National Advisory Committee for Aeronautics. NACA Rep. No. 387, 1931.

5. Ames, Milton B., Jr., and Sears, Richard I.: Pressure-Distribution Investigation of an N.A.C.A. 0009 Airfoil with a 30-Percent-Chord Plain Flap and Three Tabs. NACA TN No. 759, 1940.

6. Sears, Richard I.: Wind-Tunnel Investigation of Control-Surface Characteristics. I - Effect of Gap on the Aerodynamic Characteristics of an NACA 0009 Airfoil with a 30-Percent-Chord Plain Flap. NACA ARR, June 1941.

7. Allen, H. Julian: Calculation of the Chordwise Load Distribution over Airfoil Sections with Plain, Split, or Serially Hinged Trailing-Edge Flaps. NACA Rep. No. 634, 1938.

8. Allen, H. Julian: A Simplified Method for the Calculation of Airfoil Pressure Distribution. NACA TN No. 708, 1939.

9. Gillis, Clarence L.: Characteristics of Beveled-Trailing-Edge Elevators on a Typical Pursuit Fuselage at Attitudes Simulating Normal Flight and Spin Conditions. NACA ARR, Dec. 1942.

10. Stack, John, Lindsey, W. F., and Littell, Robert E.: The Compressibility Burble and the Effect of Compressibility on Pressures and Forces Acting on an Airfoil. NACA Rep. No. 646, 1938.

ORDINATES OF MODIFIED NACA 0009 AIRFOIL

[Stations and ordinates in percent of airfoil chord]

	Station	Ordinate
NACA 0009 airfoil section	0	0
	1.25	±1.42
	2.5	±1.96
	5.0	±2.67
	7.5	±3.15
	10	±3.51
	15	±4.01
	20	±4.30
	25	±4.46
	30	±4.50
	40	±4.35
	50	±3.97
Straight portion	60	±3.42
	70	±2.83
	80	±2.25
	90	±1.67
	100	±1.08
L.E. radius: 0.89		

TABLE II

SUMMARY OF CHARACTERISTICS OF PLAIN FLAP AND BEVELED FLAPS

Type of flap	Gap	$\left(\frac{\partial c_{h_f}}{\partial \delta_f}\right)_{\alpha_o}$	$\left(\frac{\partial c_{h_f}}{\partial \alpha_o}\right)_{\delta_f}$	$\left(\frac{\partial c_n}{\partial \alpha_o}\right)_{\delta_f}$ (Control fixed)	$\left(\frac{\partial c_n}{\partial \alpha_o}\right)_{c_{h_f}=0}$ (Control free)	$\left(\frac{\partial \alpha_o}{\partial \delta_f}\right)_{c_n}$	$\left(\frac{\partial c_m}{\partial c_n}\right)_{\delta_f}$	$\left(\frac{\partial c_m}{\partial c_n}\right)_{\alpha_o}$	$\left(\frac{\partial c_{n_f}}{\partial \delta_f}\right)_{\alpha_o}$	$\left(\frac{\partial c_{n_f}}{\partial \alpha_o}\right)_{\delta_f}$
Plain	Sealed	-0.0120	-0.0065	0.098	0.066	-0.60	0.010	-0.151	0.039	0.022
	0.005c	-.0118	-.0066	.096	.066	-.56	.010	-.151	-------	--------
$0.15c_f$ bevel	Sealed	-0.0054	0.0015	0.088	0.102	-0.56	0.026	-0.150	0.030	0.008
	0.005c	-.0016	.0030	.082	.154	-.47	.039	-.148	.027	.006
$0.20c_f$ bevel	Sealed	-0.0068	-0.0006	0.092	0.087	-0.57	0.029	-0.164	0.031	0.009
	0.005c	-.0035	.0002	.087	.089	-.47	.034	-.157	.029	.010
$0.15c_f$ bevel (small radius)	Sealed	-0.0030	0.0007	0.091	0.102	-0.52	0.024	-0.154	0.030	0.008
	0.005c	-.0005	.0030	.085	.320	-.46	.031	-.142	.027	.007

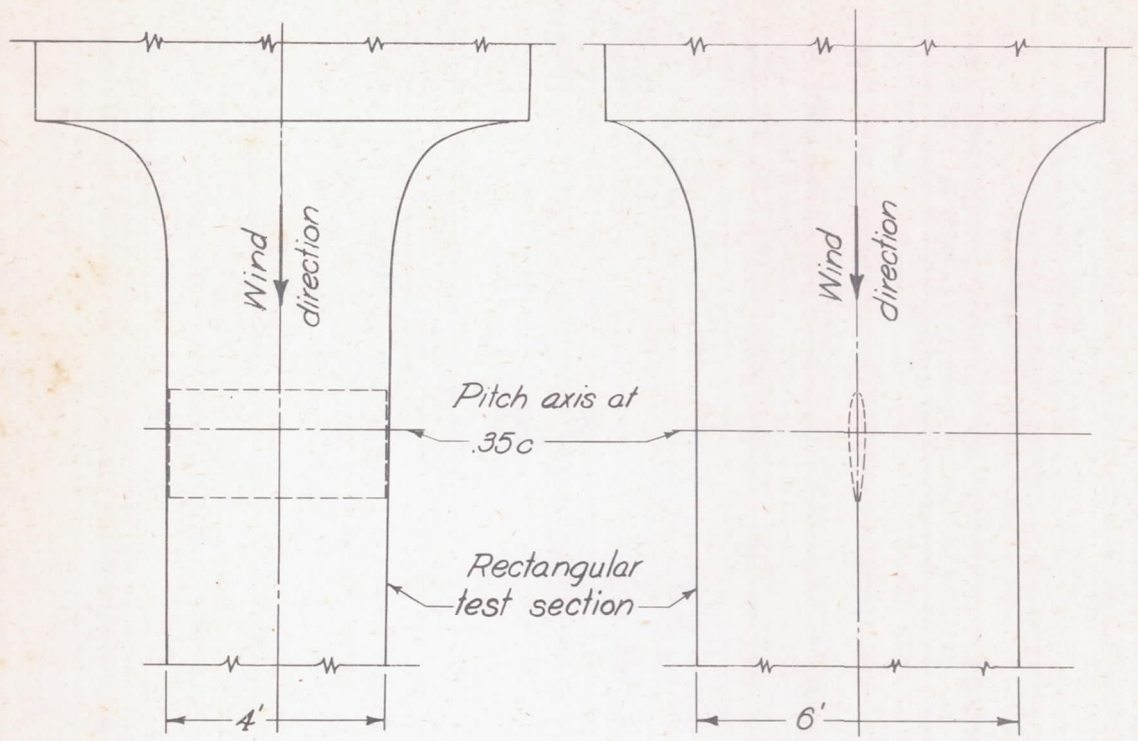

Model mounted in NACA 4-by 6-foot vertical tunnel

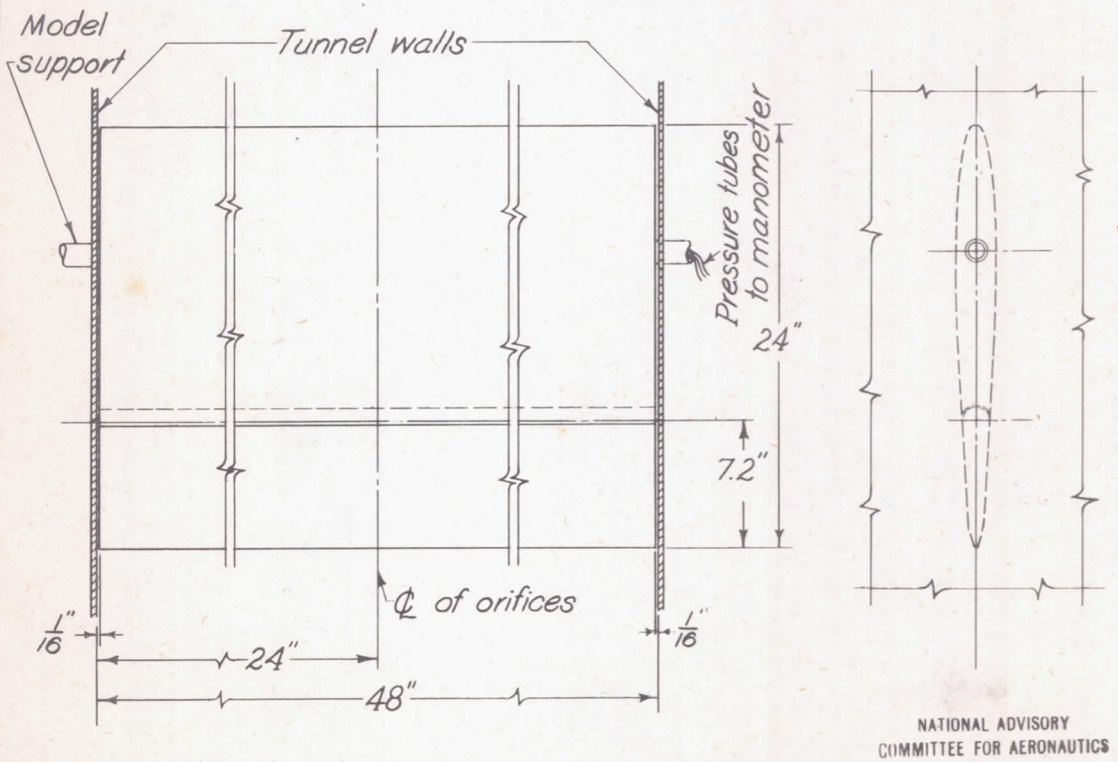

Figure 1.-Installation of beveled-trailing-edge pressure-distribution model in NACA 4-by 6-foot vertical tunnel.

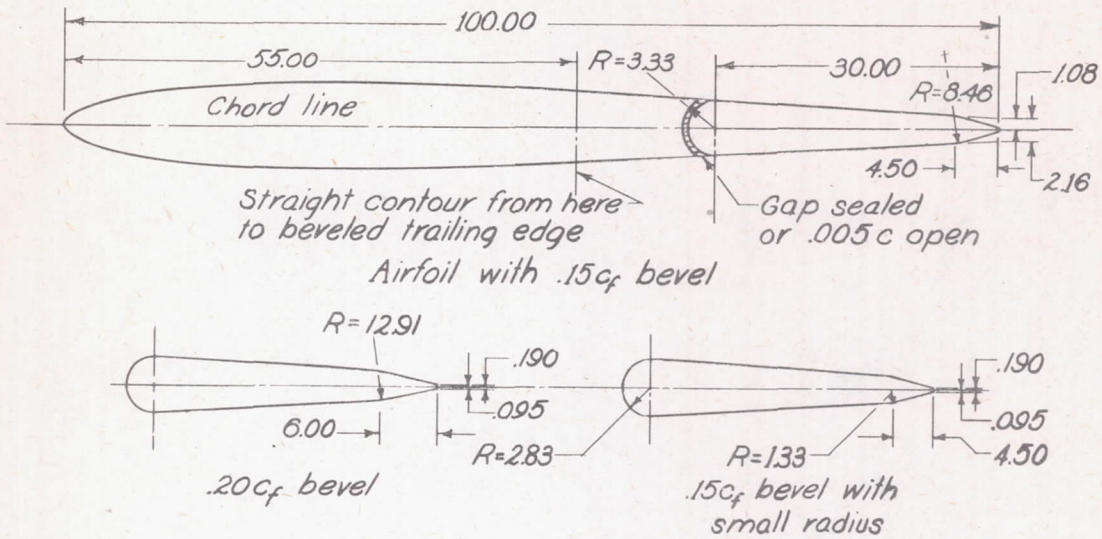

(a) Two-foot-chord NACA 0009 airfoil model with a 0.30c plain flap having 0.15c_f and 0.20c_f beveled trailing edges. Dimensions are in percent of airfoil chord.

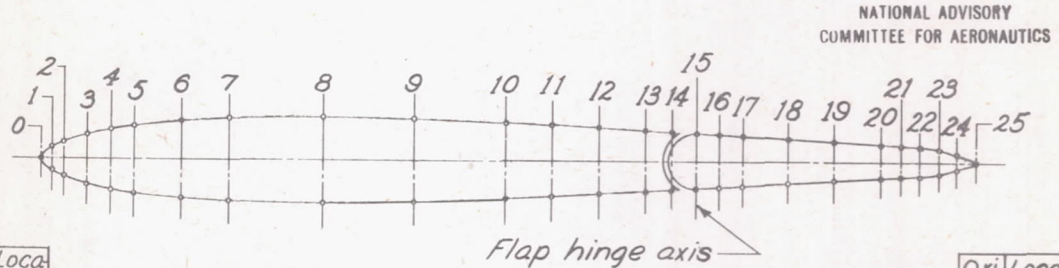

Orifice	Location
0	0
1	1.25
2	2.50
3	5.00
4	7.50
5	10.00
6	15.00
7	20.00
8	30.00
9	40.00
10	50.00
11	55.00
12	60.00

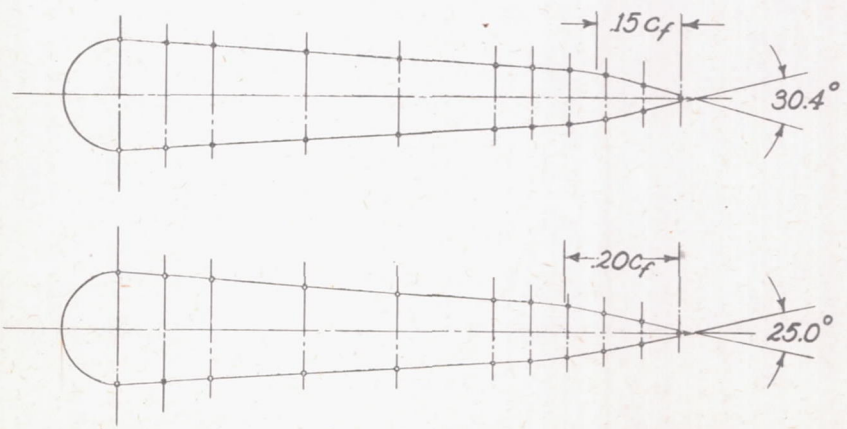

Orifice	Location
13	65.00
14	67.50
15	70.00
16	72.50
17	75.00
18	80.00
19	85.00
20	90.00
21	92.00
22	94.00
23	96.00
24	98.00
25	100.00

(b) Chordwise locations of pressure orifices on airfoil and on the flaps having 0.15c_f and 0.20c_f bevels.

Figure 2.-Dimensions and chordwise pressure-orifice locations for NACA 0009 beveled-trailing-edge pressure-distribution model. Dimensions and orifice locations are in percent of airfoil chord.

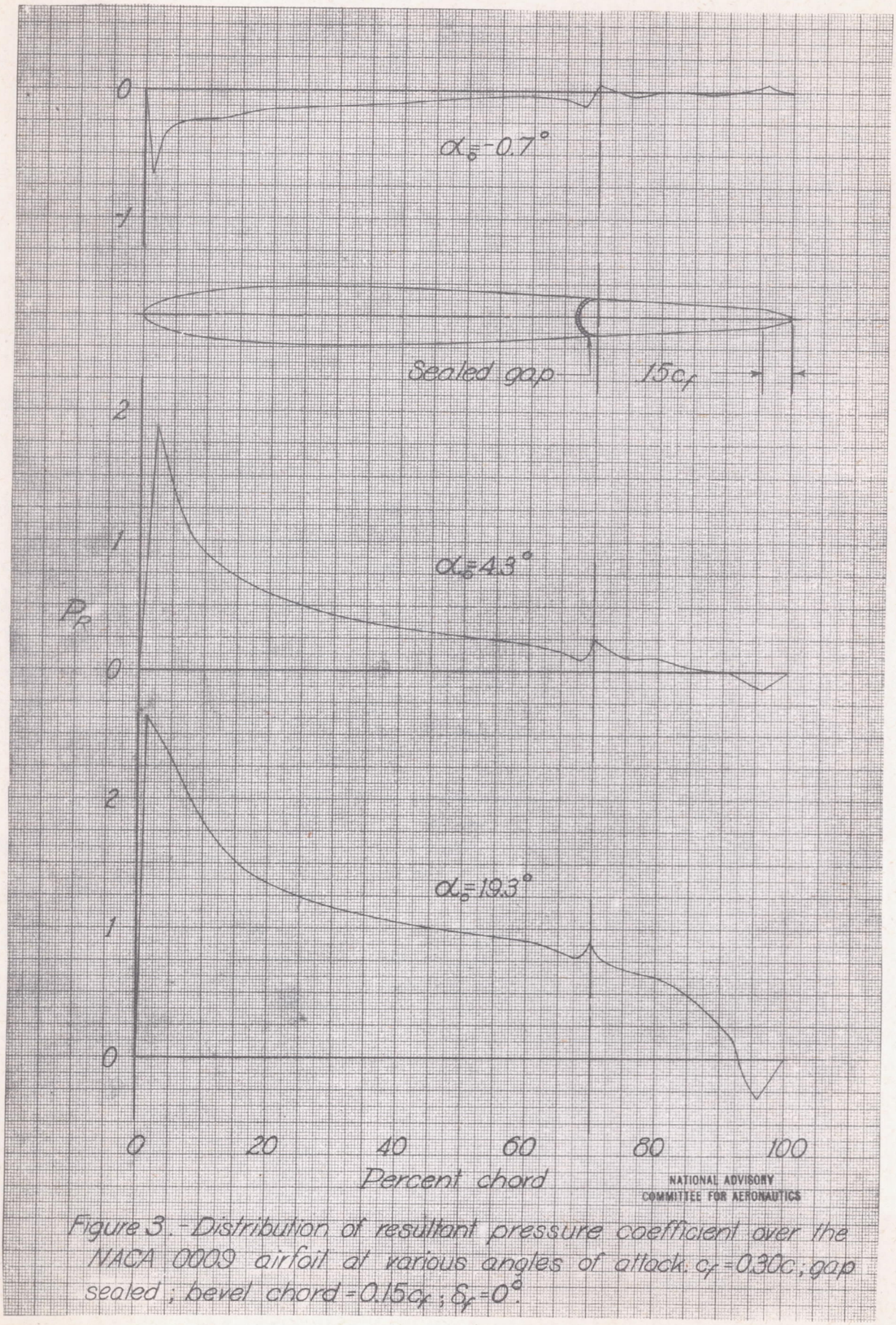

Figure 3.- Distribution of resultant pressure coefficient over the NACA 0009 airfoil at various angles of attack. c_f=0.30c; gap sealed; bevel chord=0.15c_f; δ_f=0°.

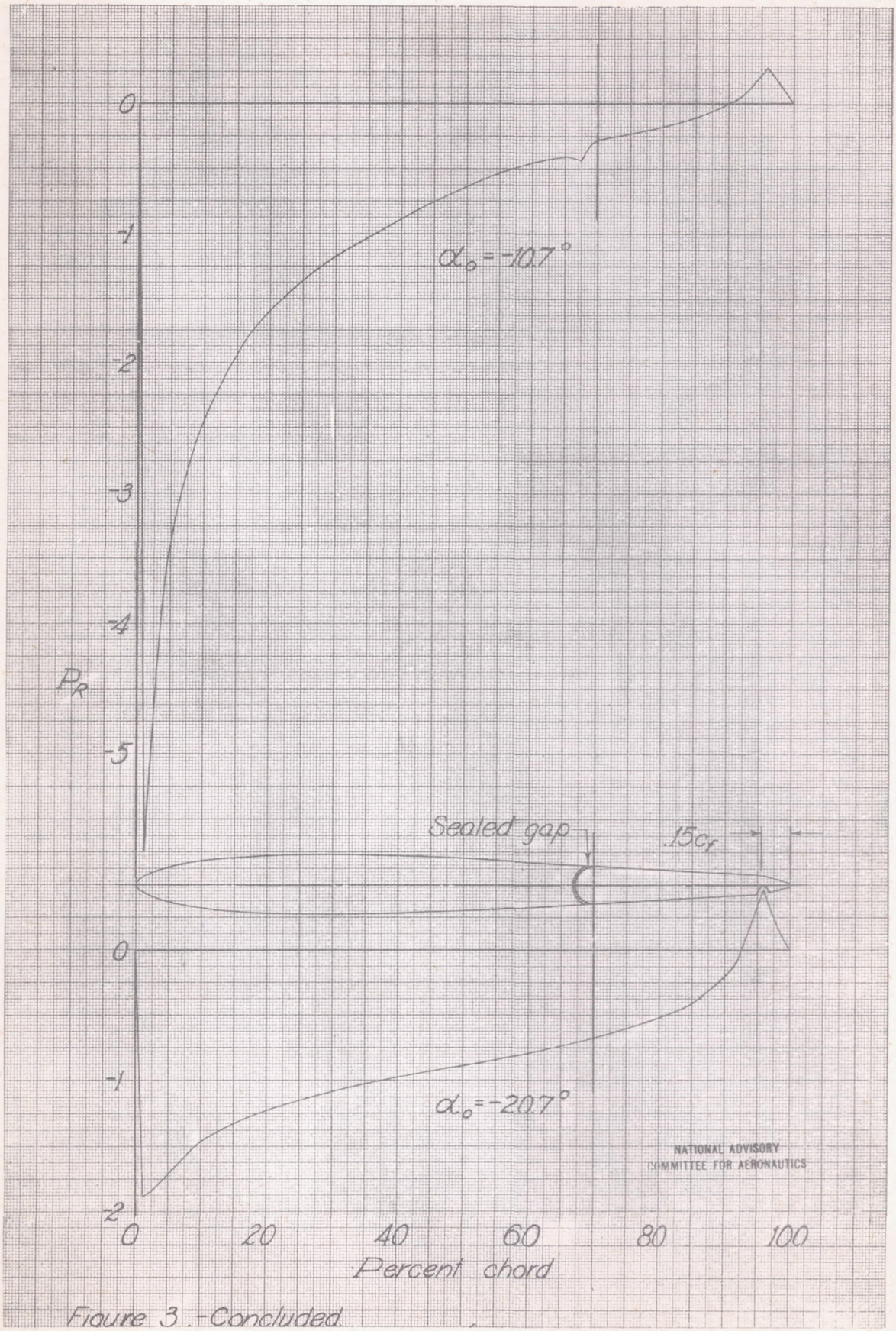

Figure 3.- Concluded

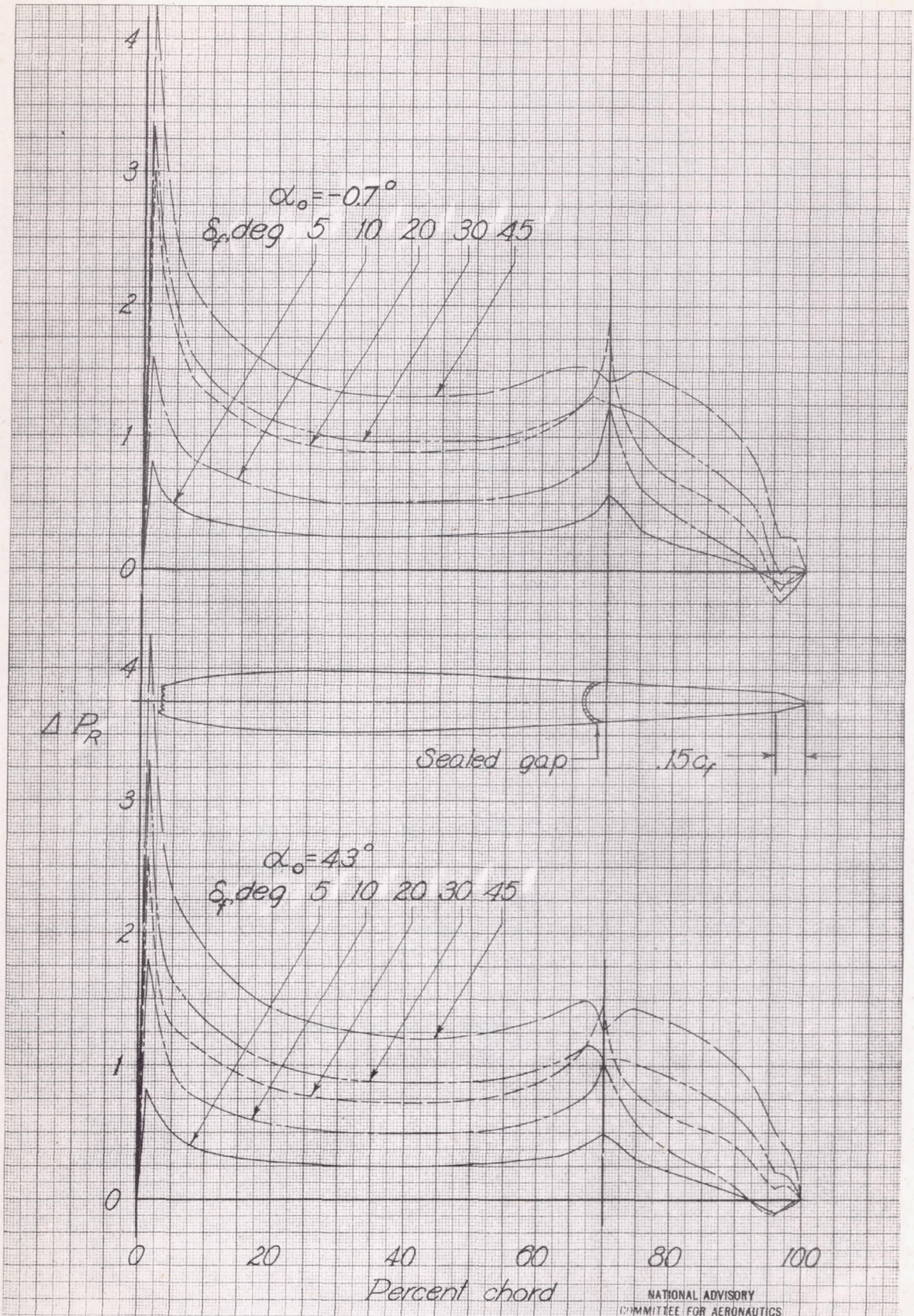

Figure 4.- Increments of resultant pressure coefficient over the NACA 0009 airfoil for various flap deflections at several angles of attack. $c_f = 0.30c$; gap sealed; bevel chord = $0.15\,c_f$.

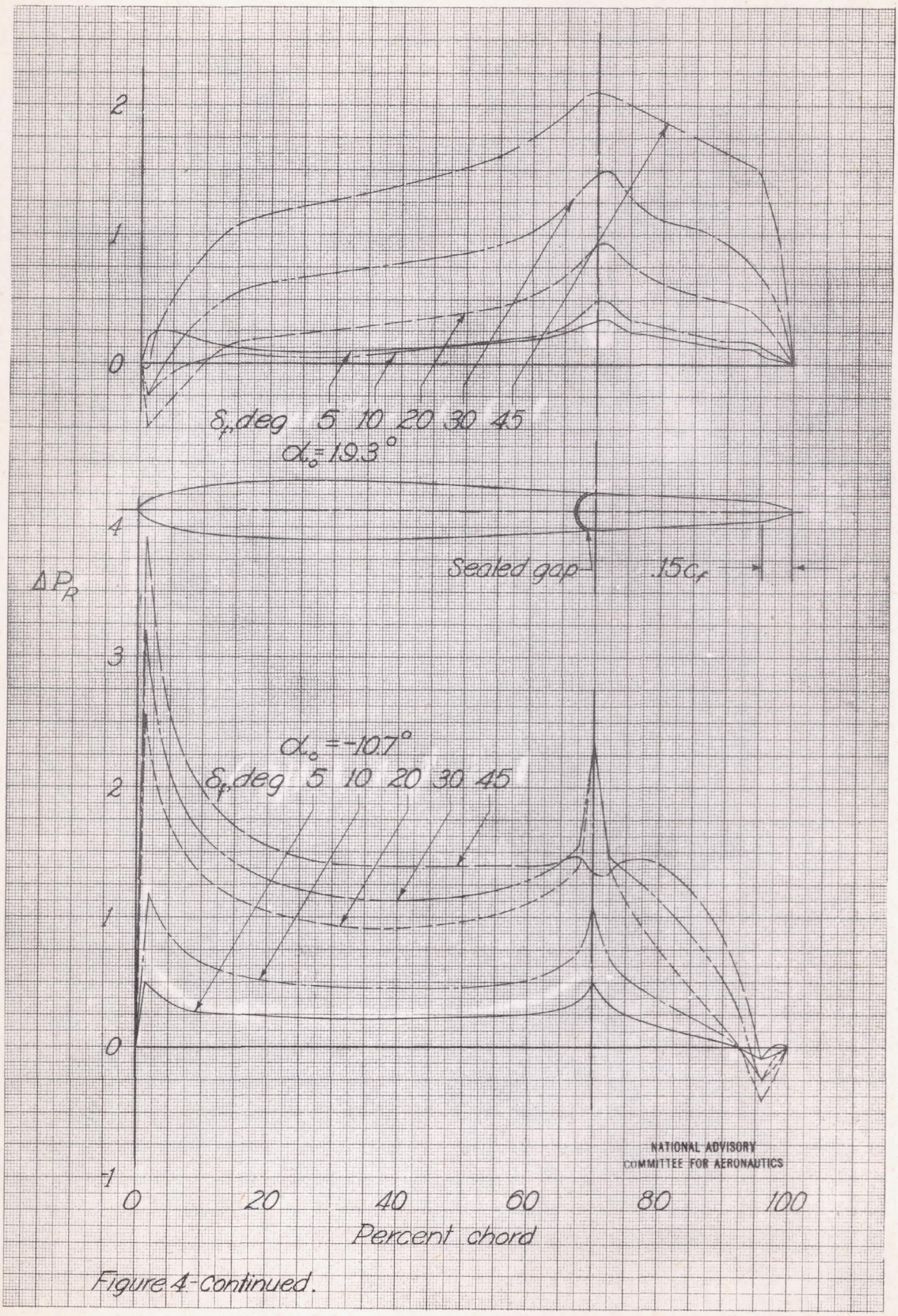

Figure 4.-Continued.

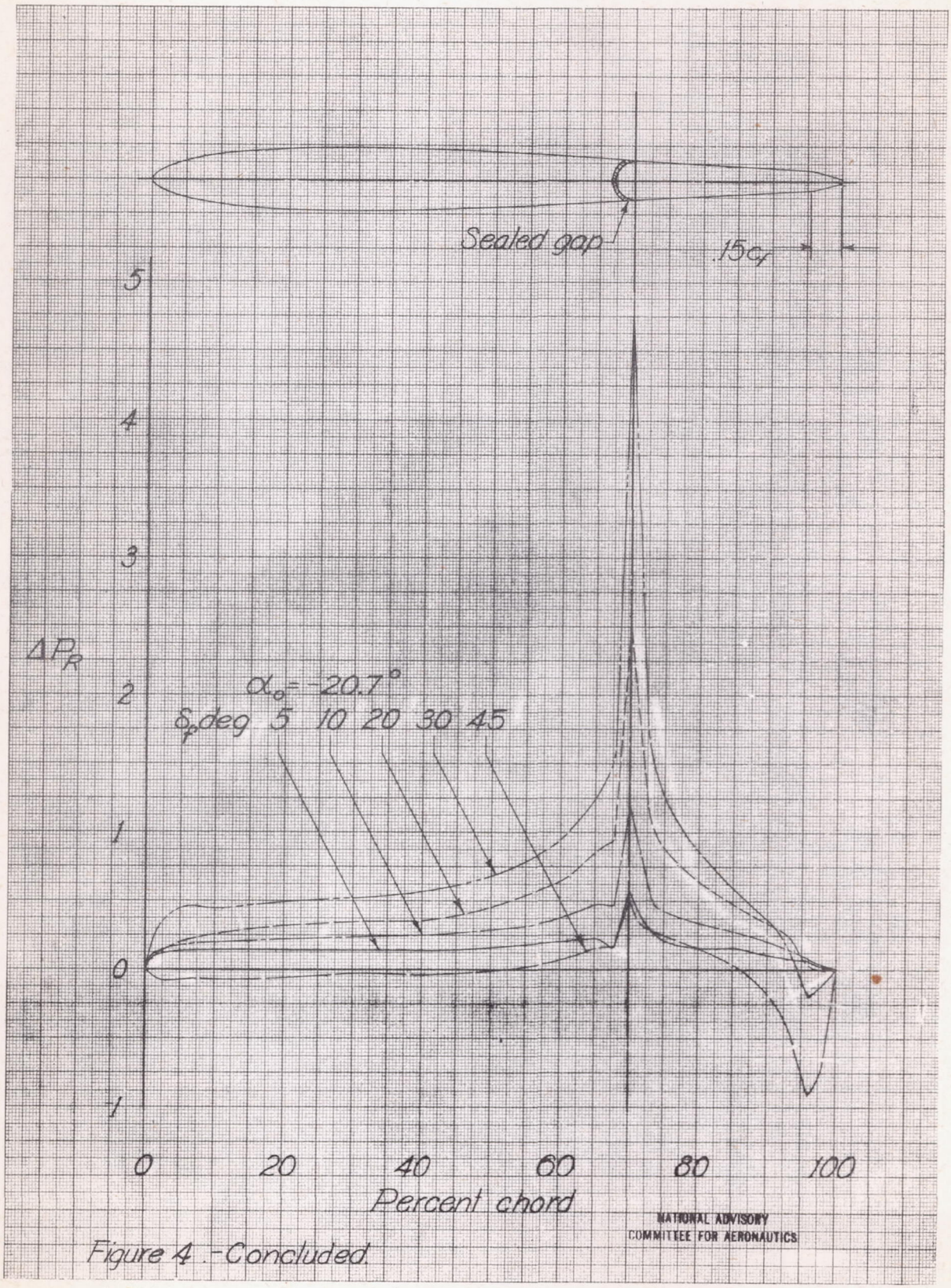

Figure 4.- Concluded.

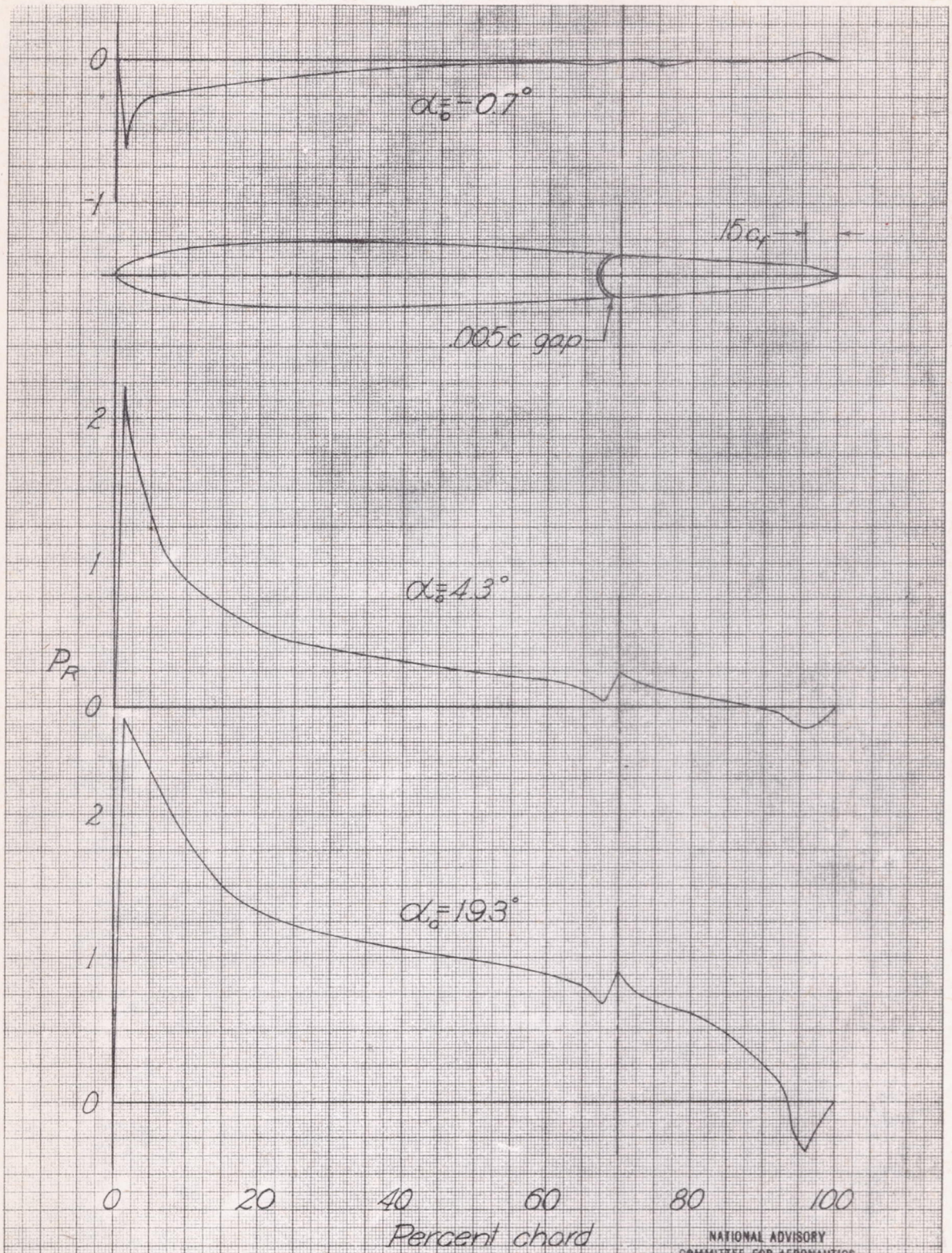

Figure 5.- Distribution of resultant pressure coefficient over the NACA 0009 airfoil at various angles of attack. $c_f = 0.30c$; gap = 0.005c; bevel chord = $0.15c_f$; $\delta_f = 0°$.

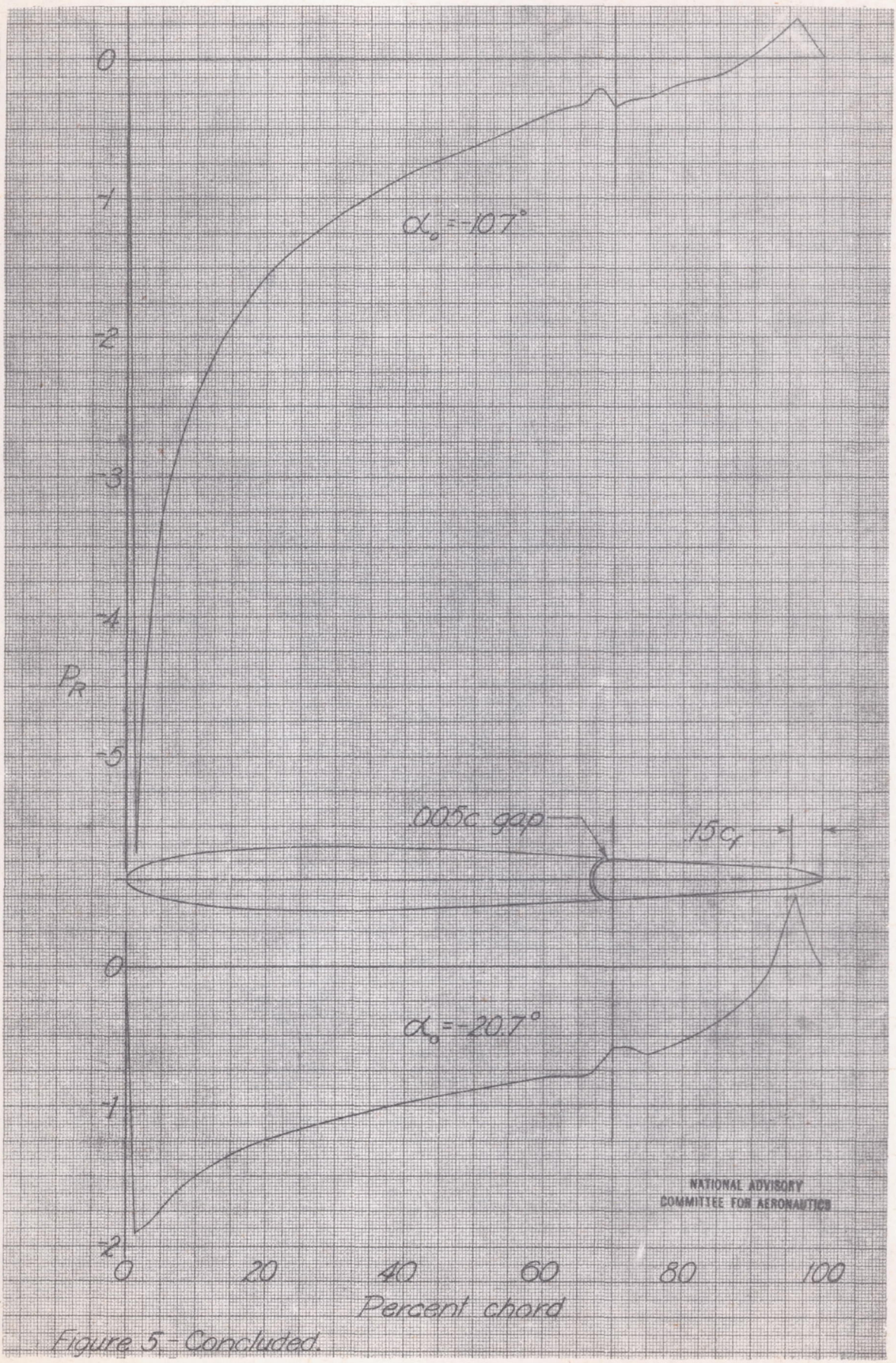

Figure 5 - Concluded.

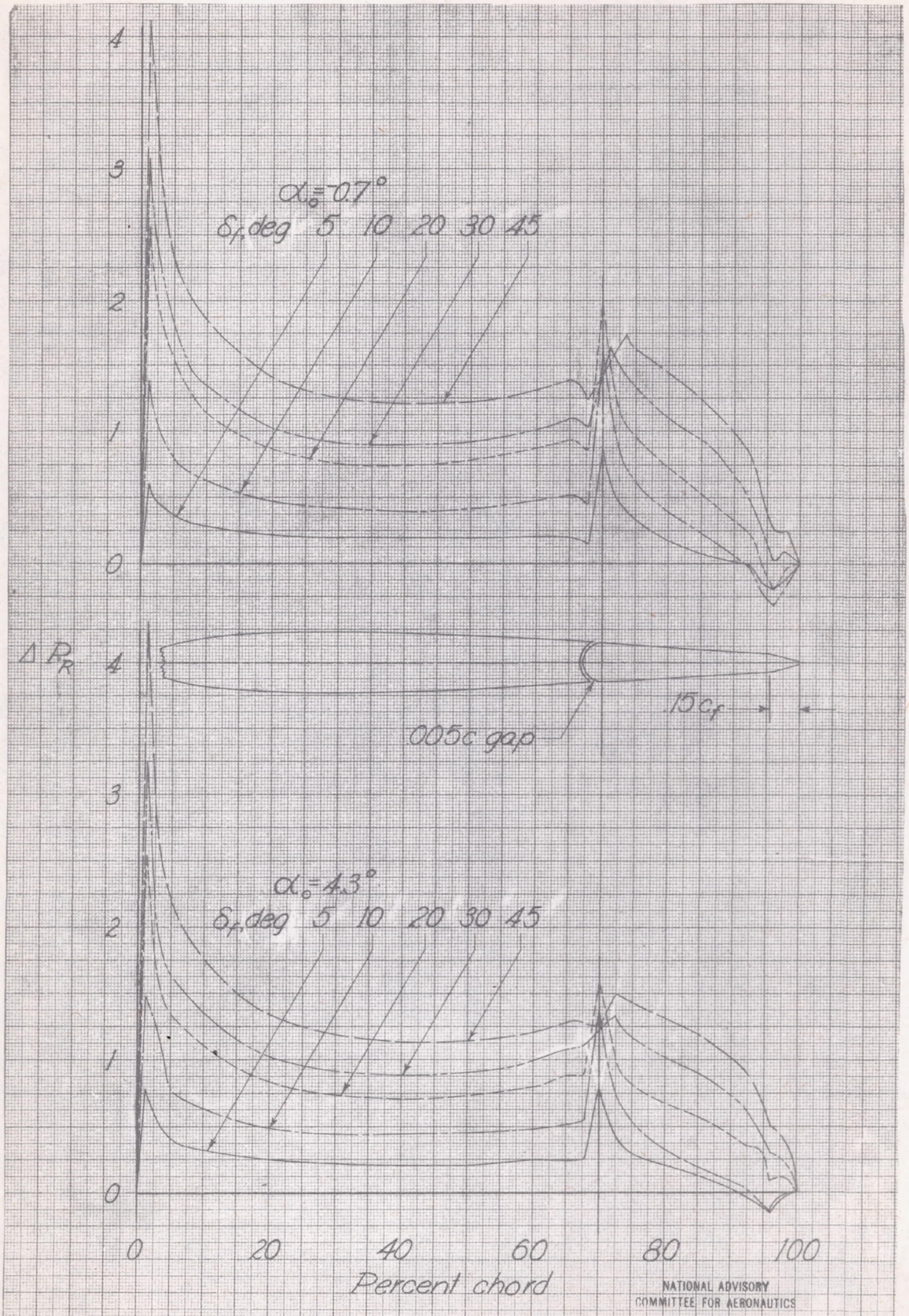

Figure 6.-Increments of resultant pressure coefficient over the NACA 0009 airfoil for various flap deflections at several angles of attack. c_f=0.30c; gap=0.005c; bevel chord=0.15c_f.

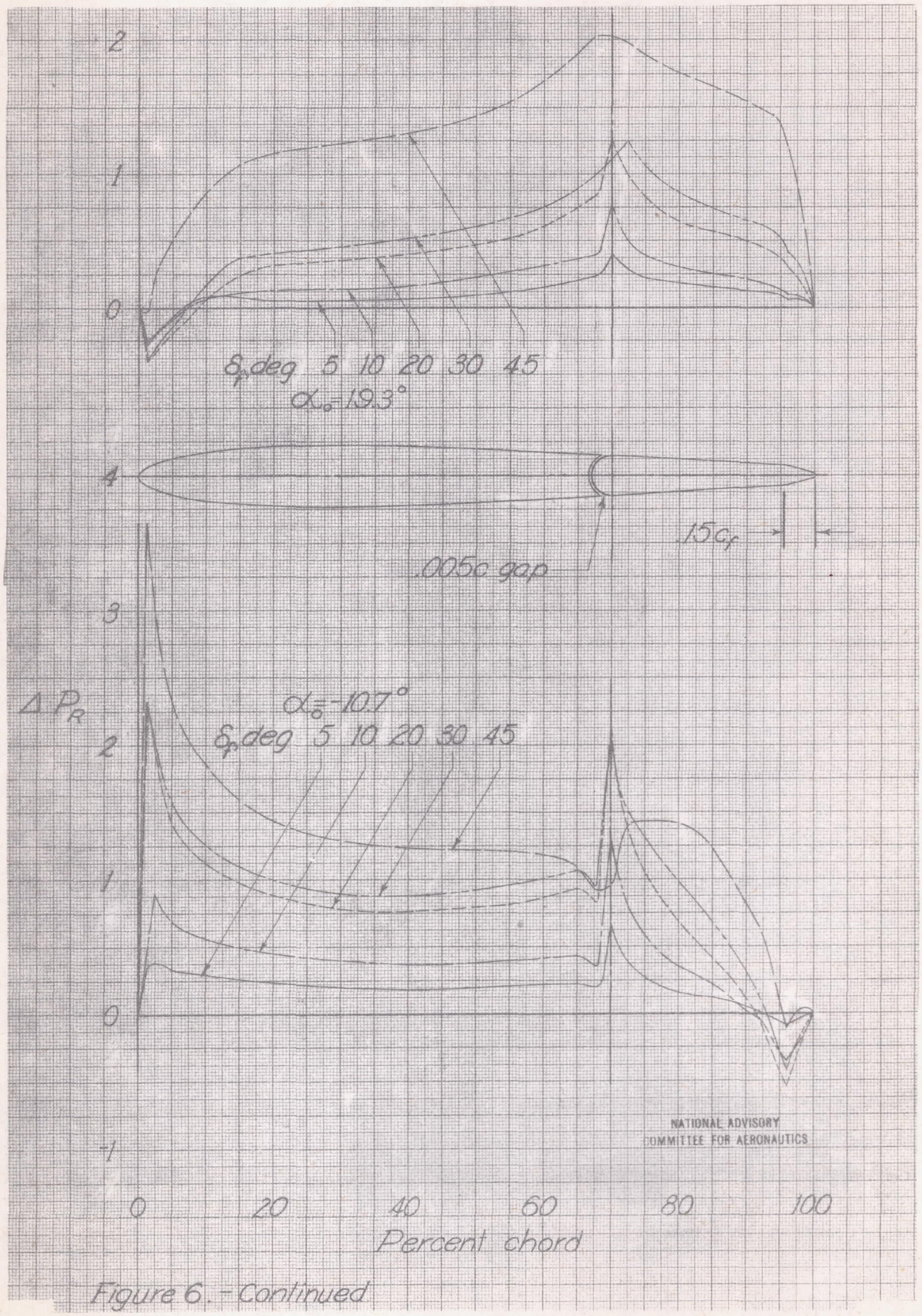

Figure 6. - Continued

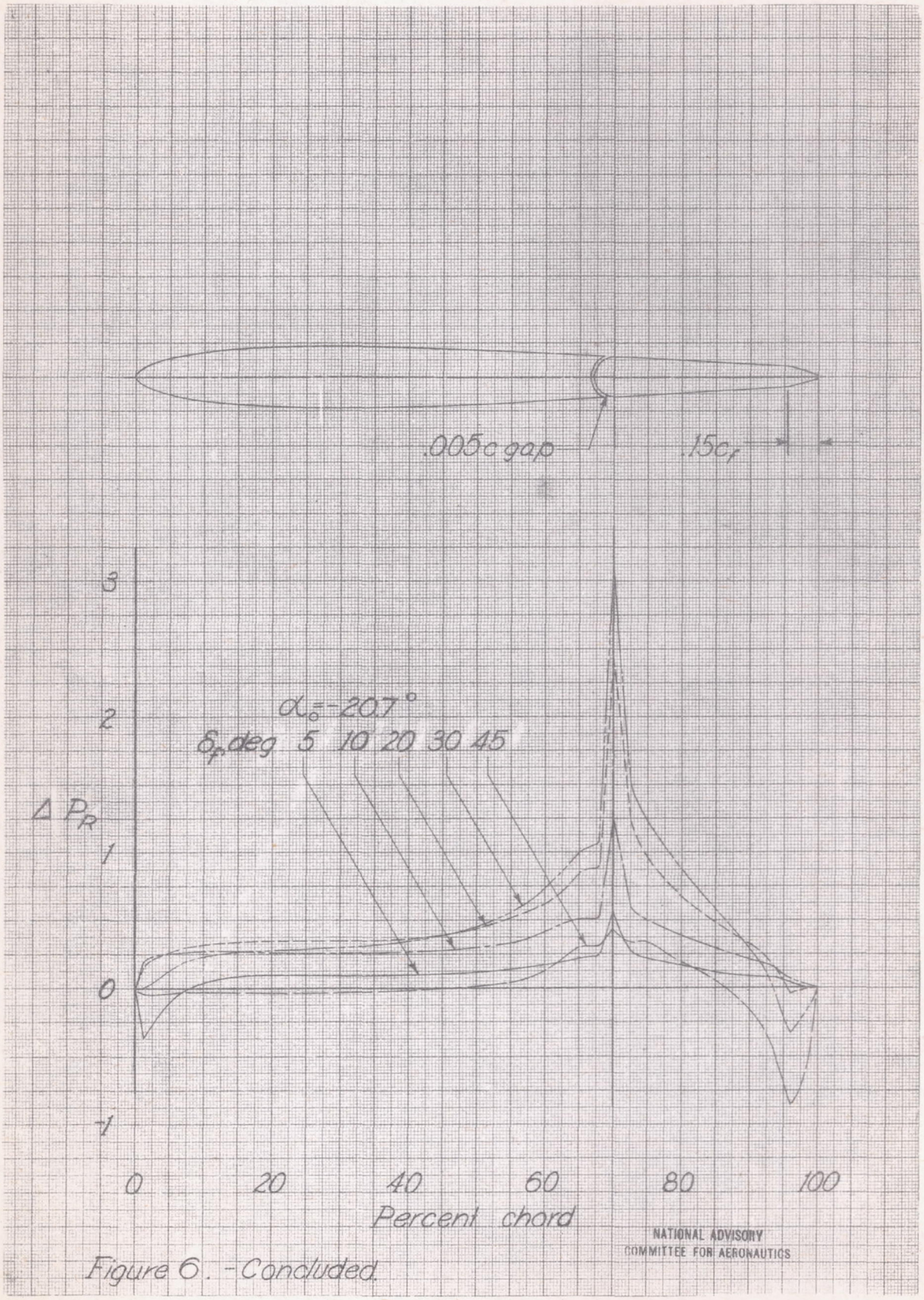

Figure 6. - Concluded.

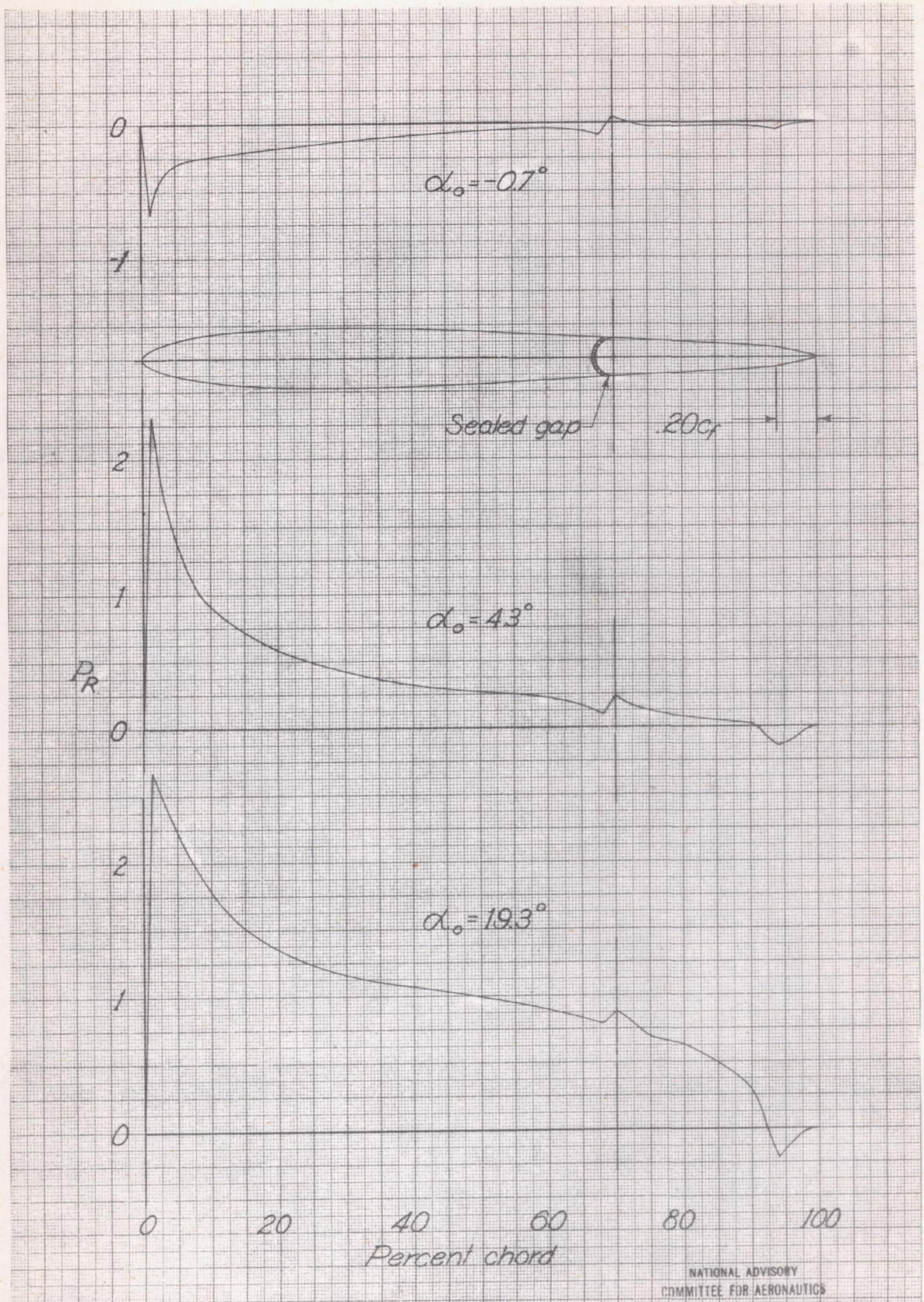

Figure 7.- Distribution of resultant pressure coefficient over the NACA 0009 airfoil at various angles of attack. $c_f = 0.30c$; gap sealed; bevel chord $= 0.20c_f$; $\delta_f = 0°$.

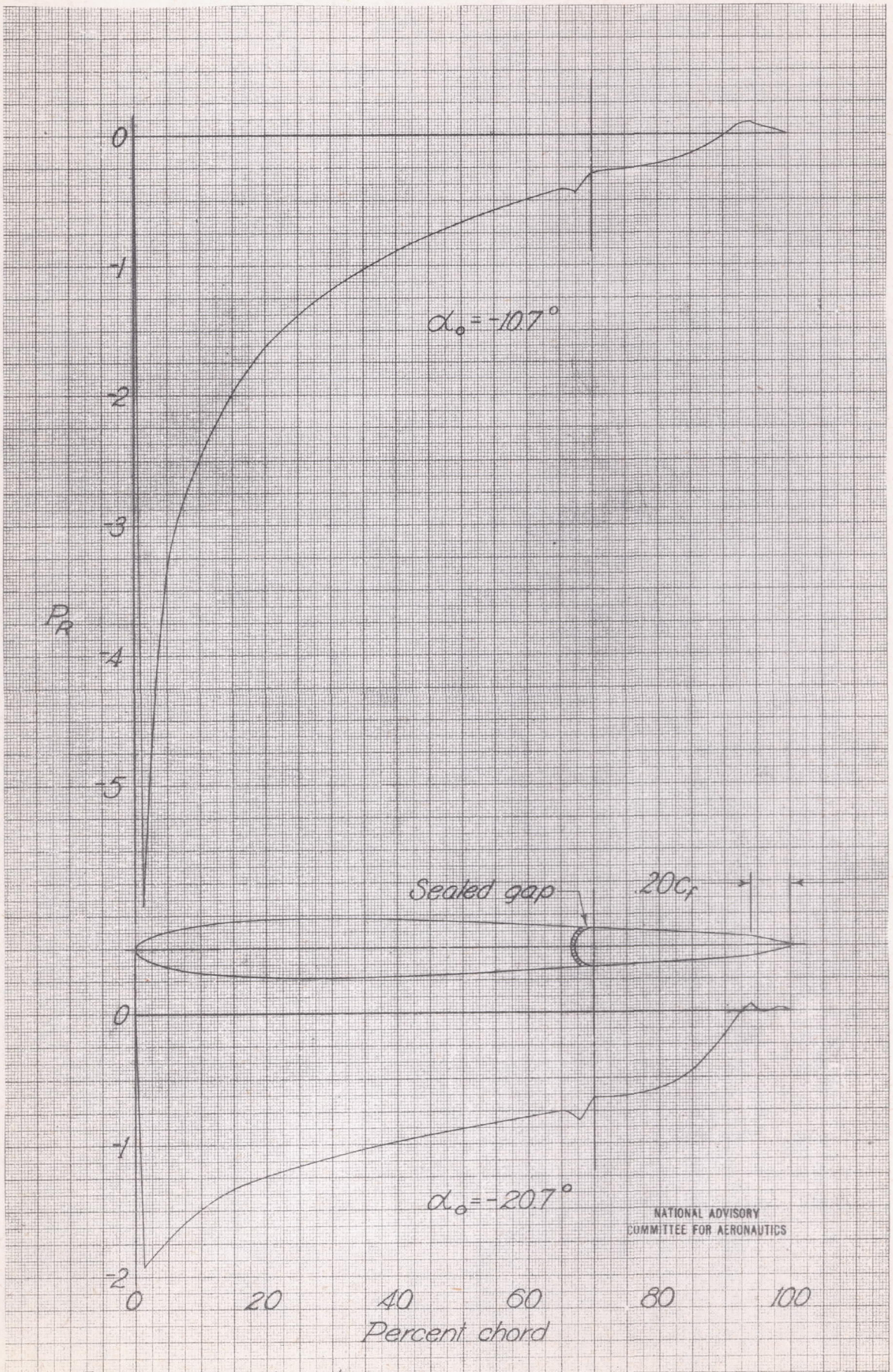

Figure 7.- Concluded.

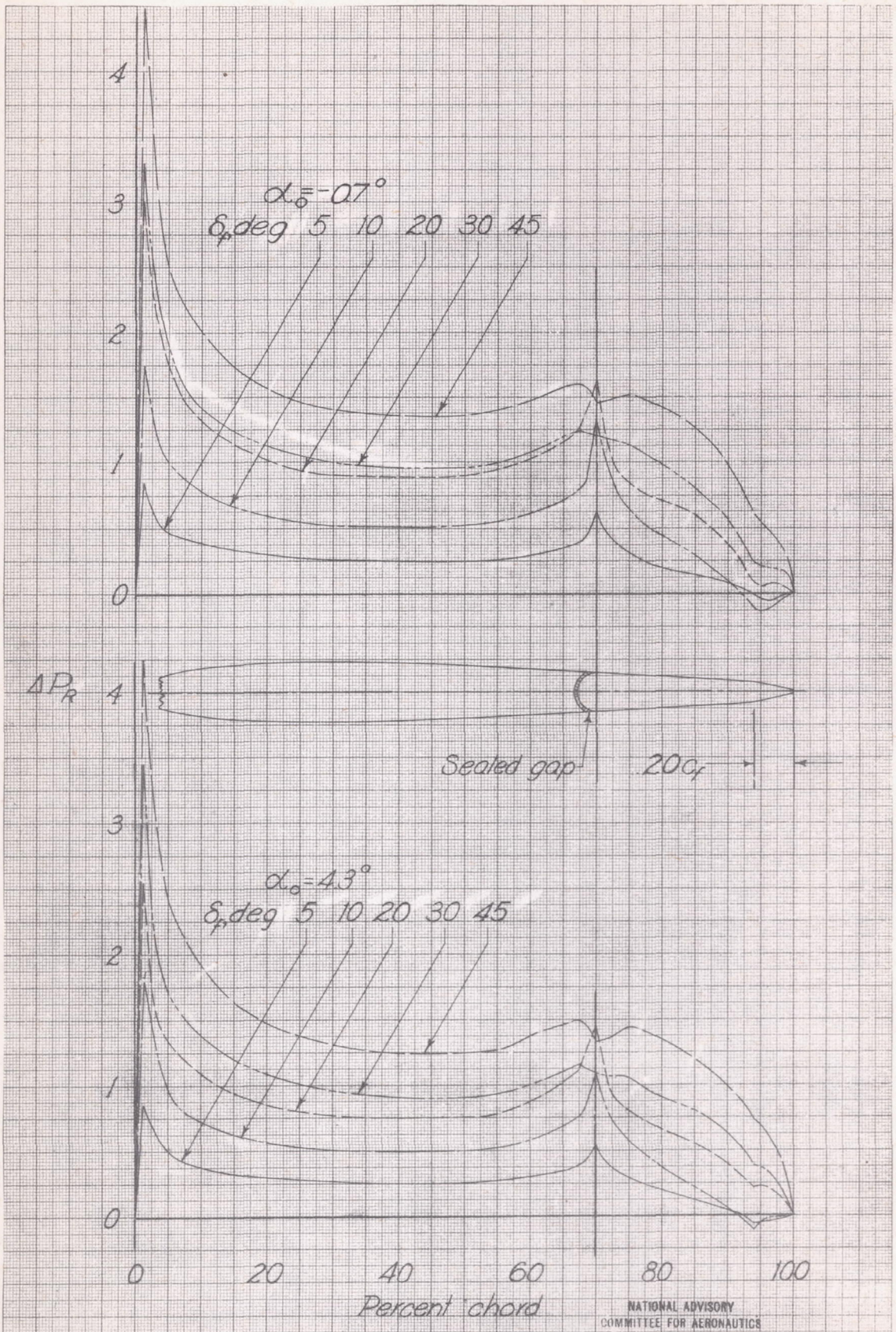

Figure 8.- Increments of resultant pressure coefficient over the NACA 0009 airfoil for various flap deflections at several angles of attack. c_f=0.30c; sealed gap; bevel chord=0.20c_f.

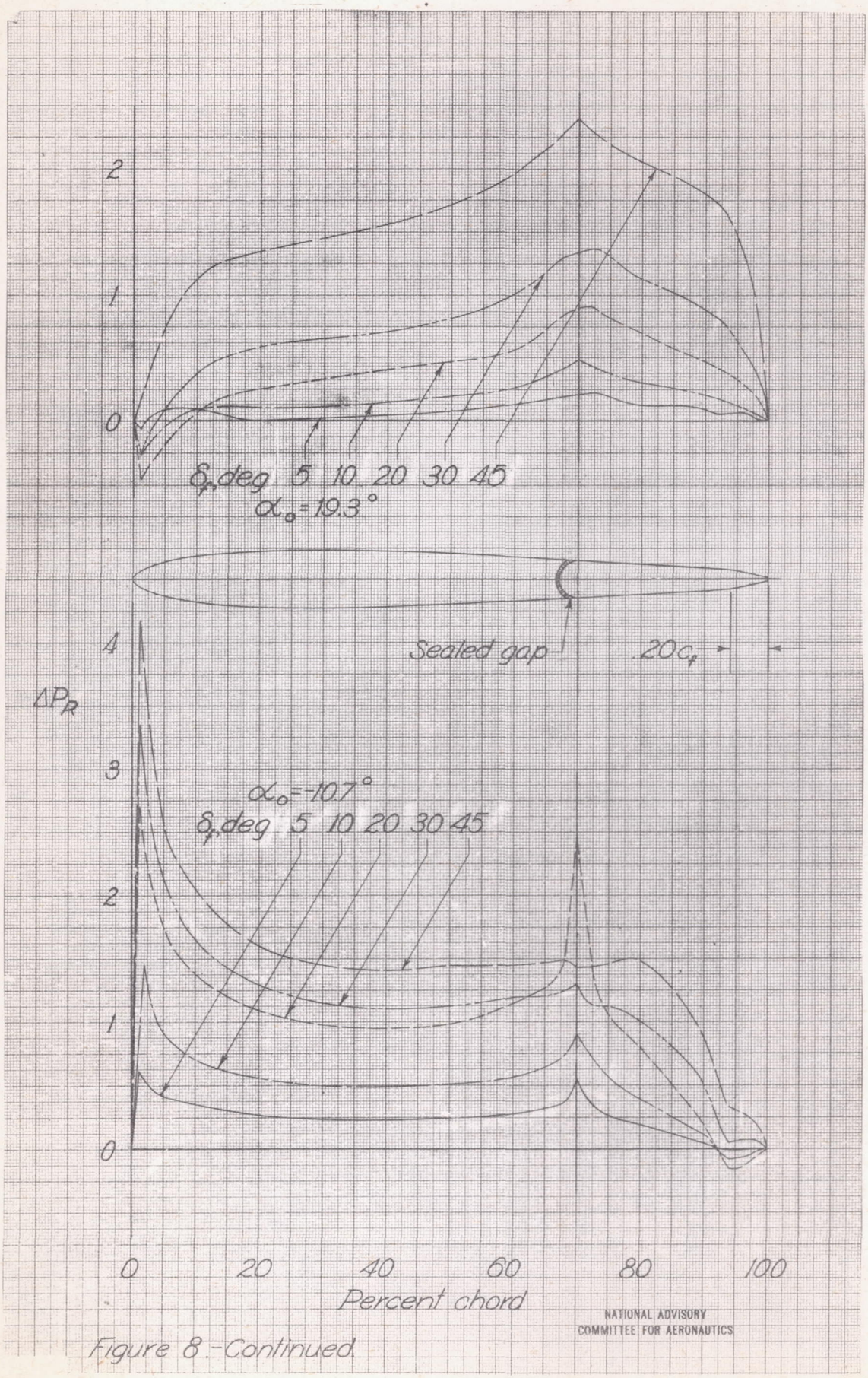

Figure 8.-Continued.

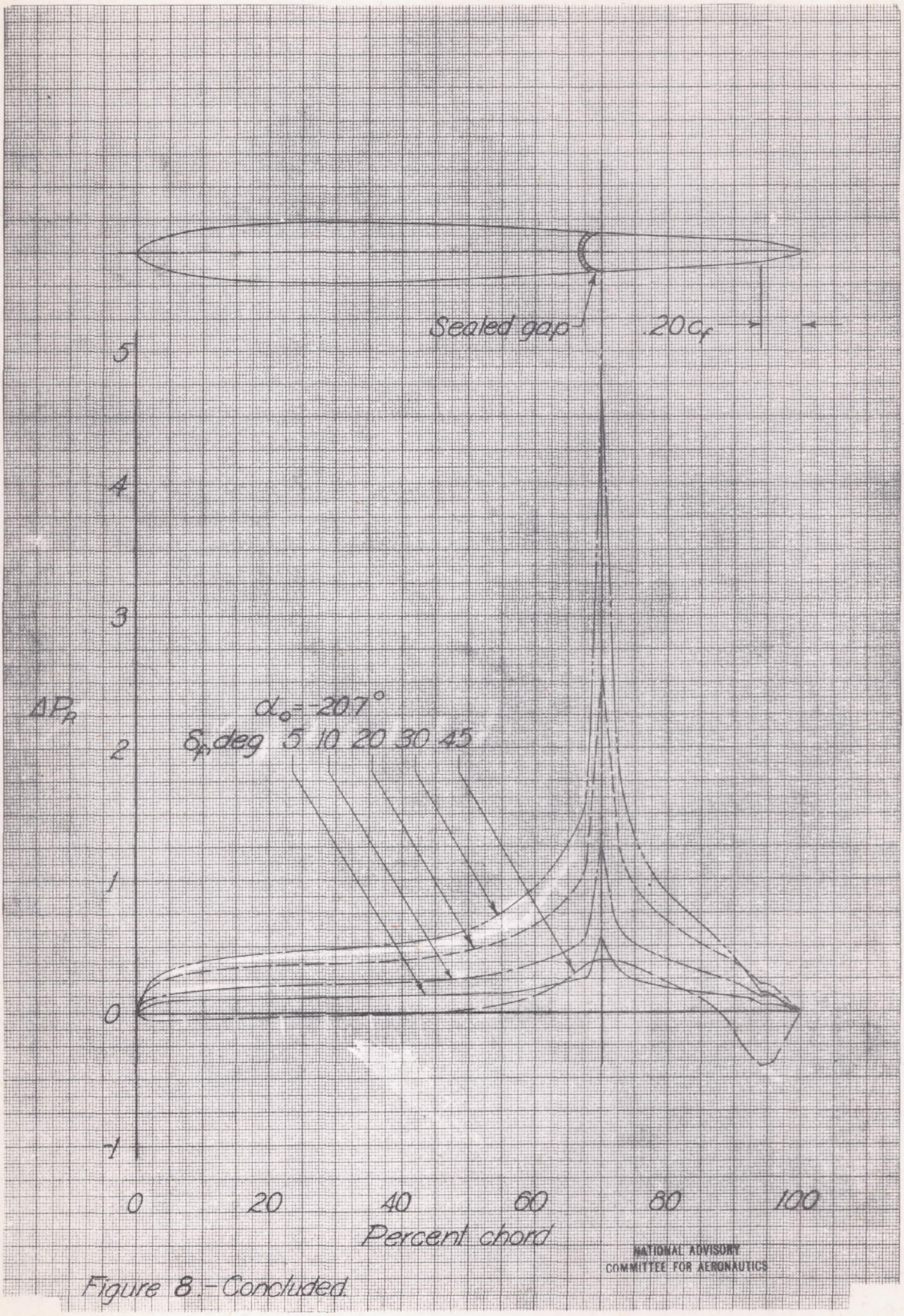

Figure 8.- Concluded.

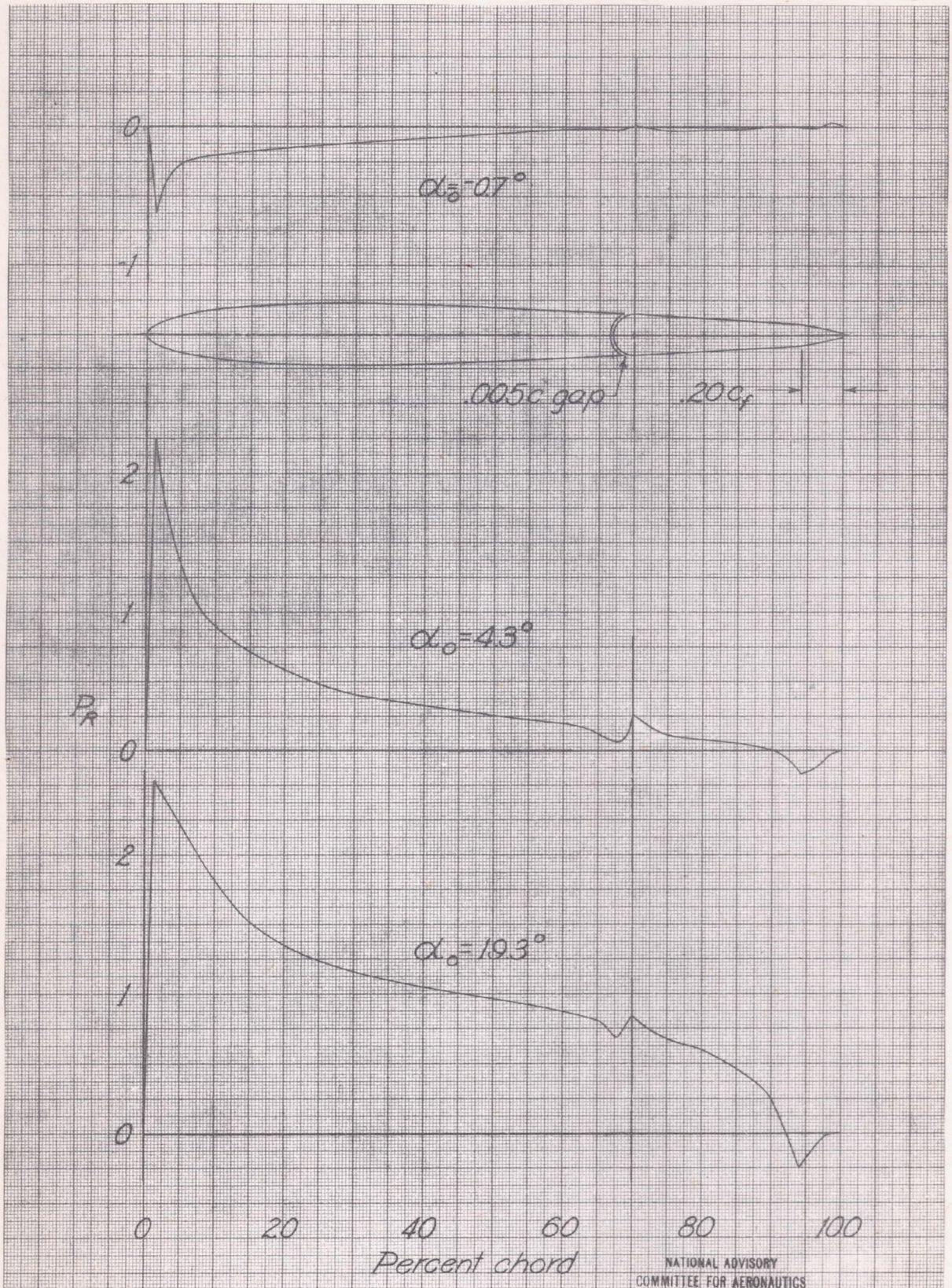

Figure 9.- Distribution of resultant pressure coefficient over the NACA 0009 airfoil at various angles of attack. c_f = 0.30c; gap = 0.005c; bevel chord = 0.20c_f; δ_f = 0°.

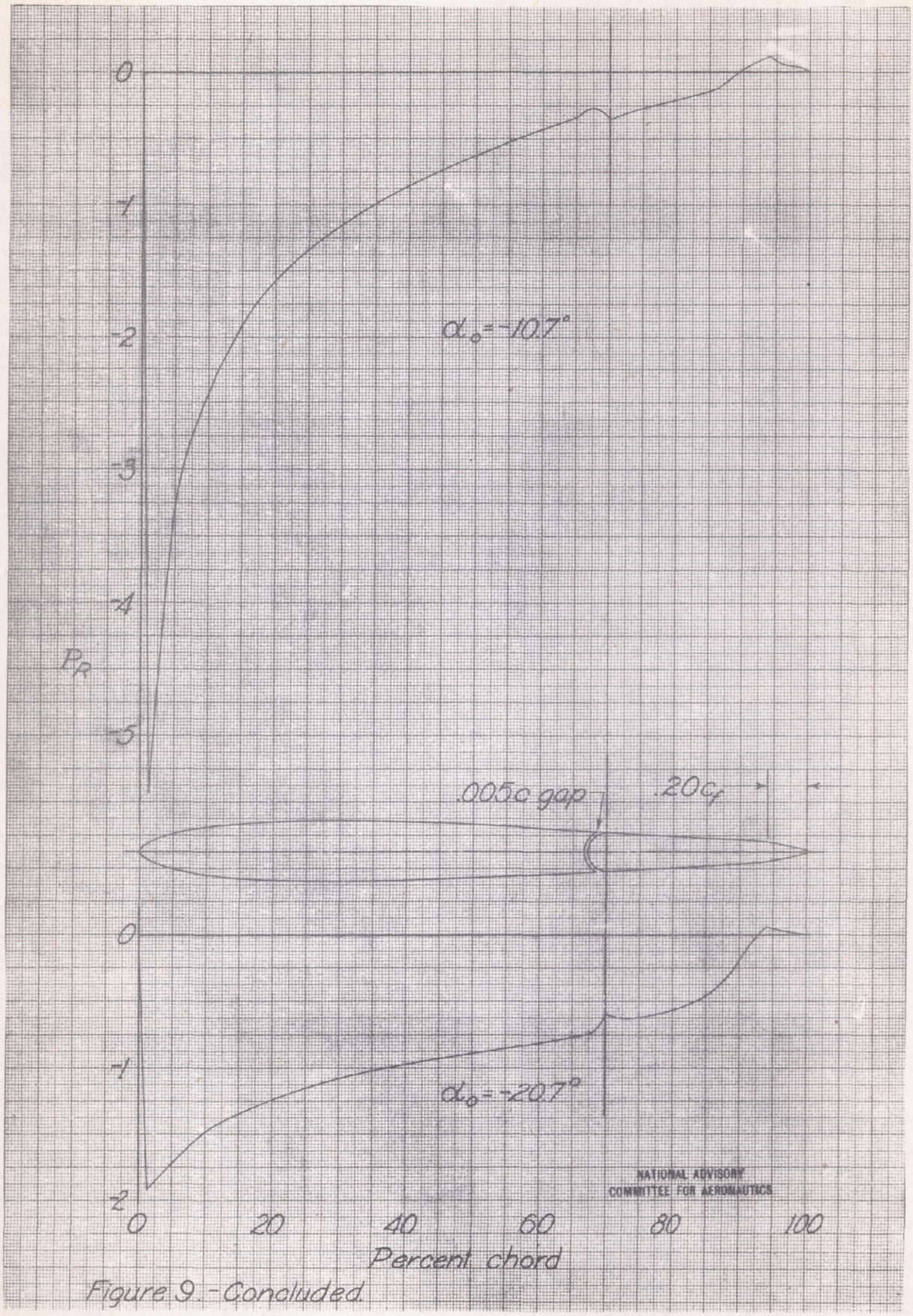

Figure 9.- Concluded.

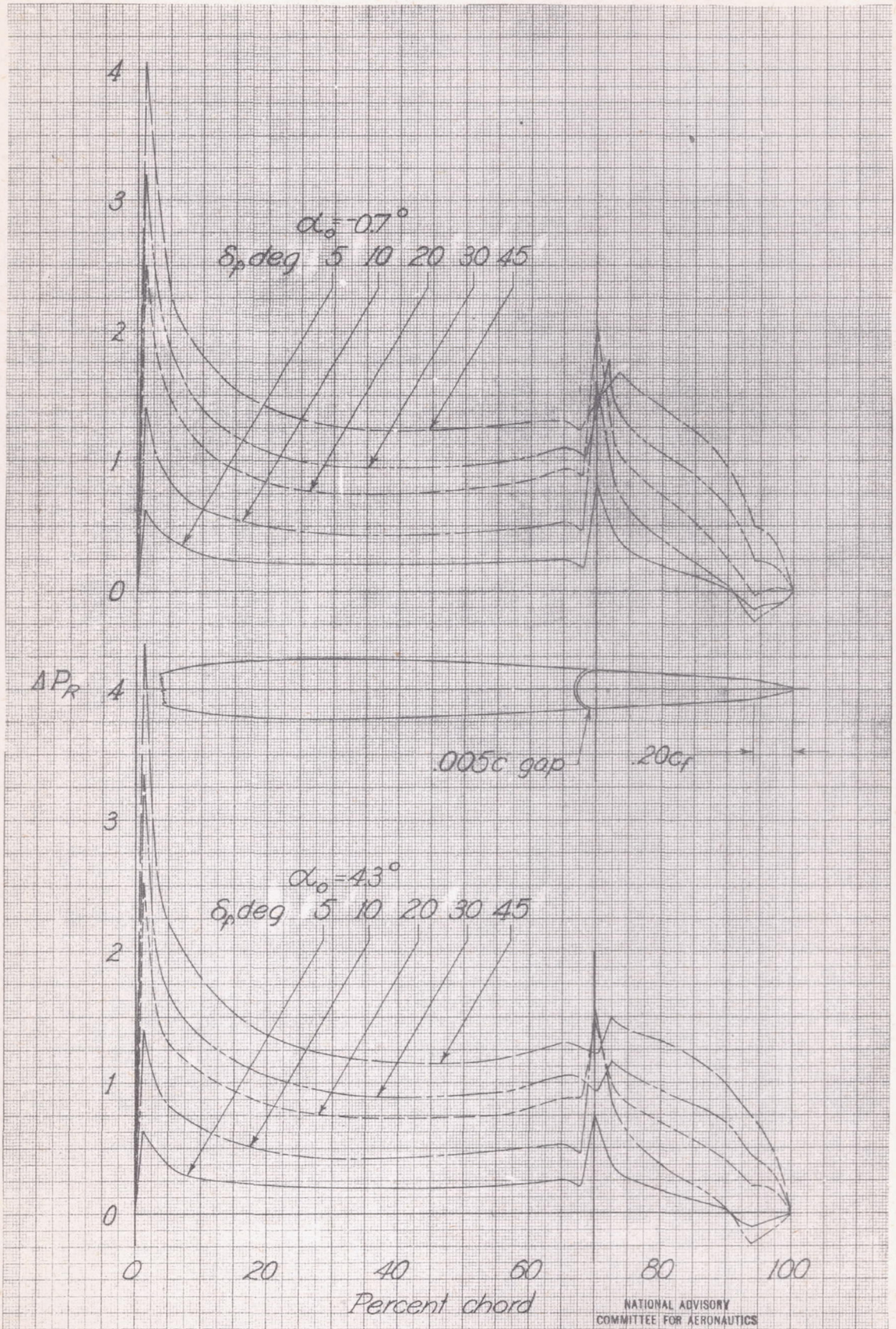

Figure 10.- Increments of resultant pressure coefficient over the NACA 0009 airfoil for various flap deflections at several angles of attack. c_f=0.30c; gap=.005c; bevel chord=0.20c_f

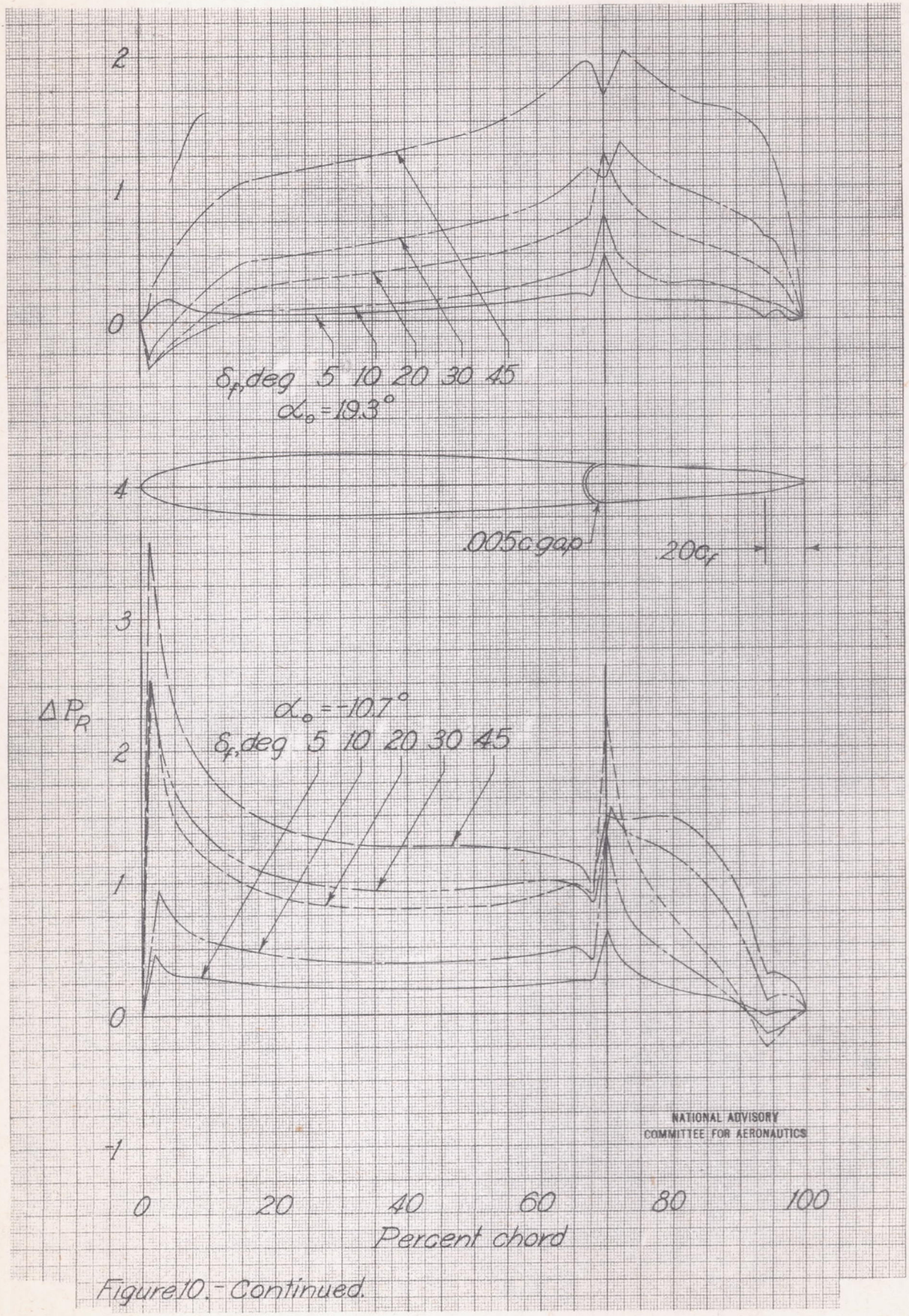

Figure 10.- Continued.

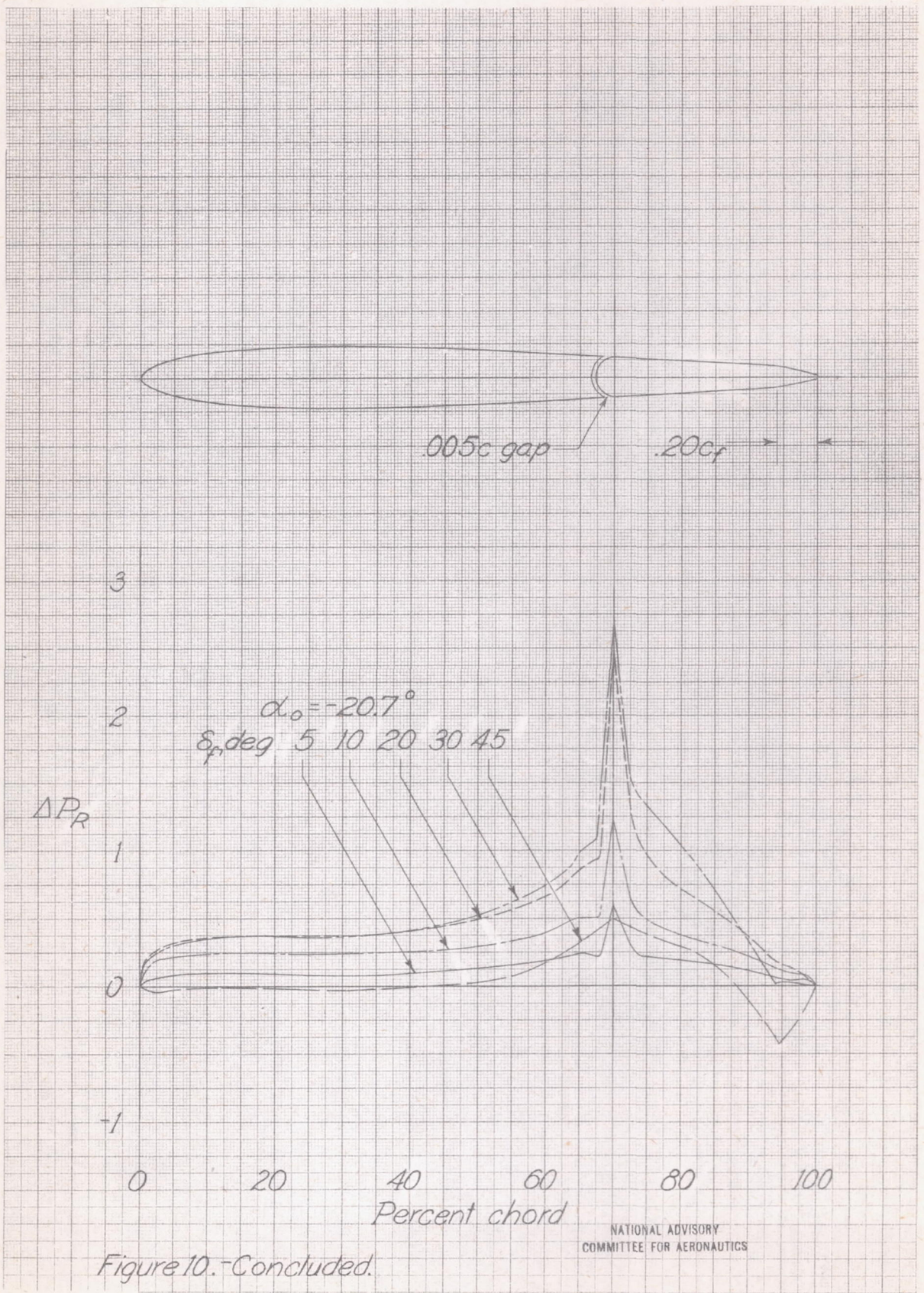

Figure 10.- Concluded.

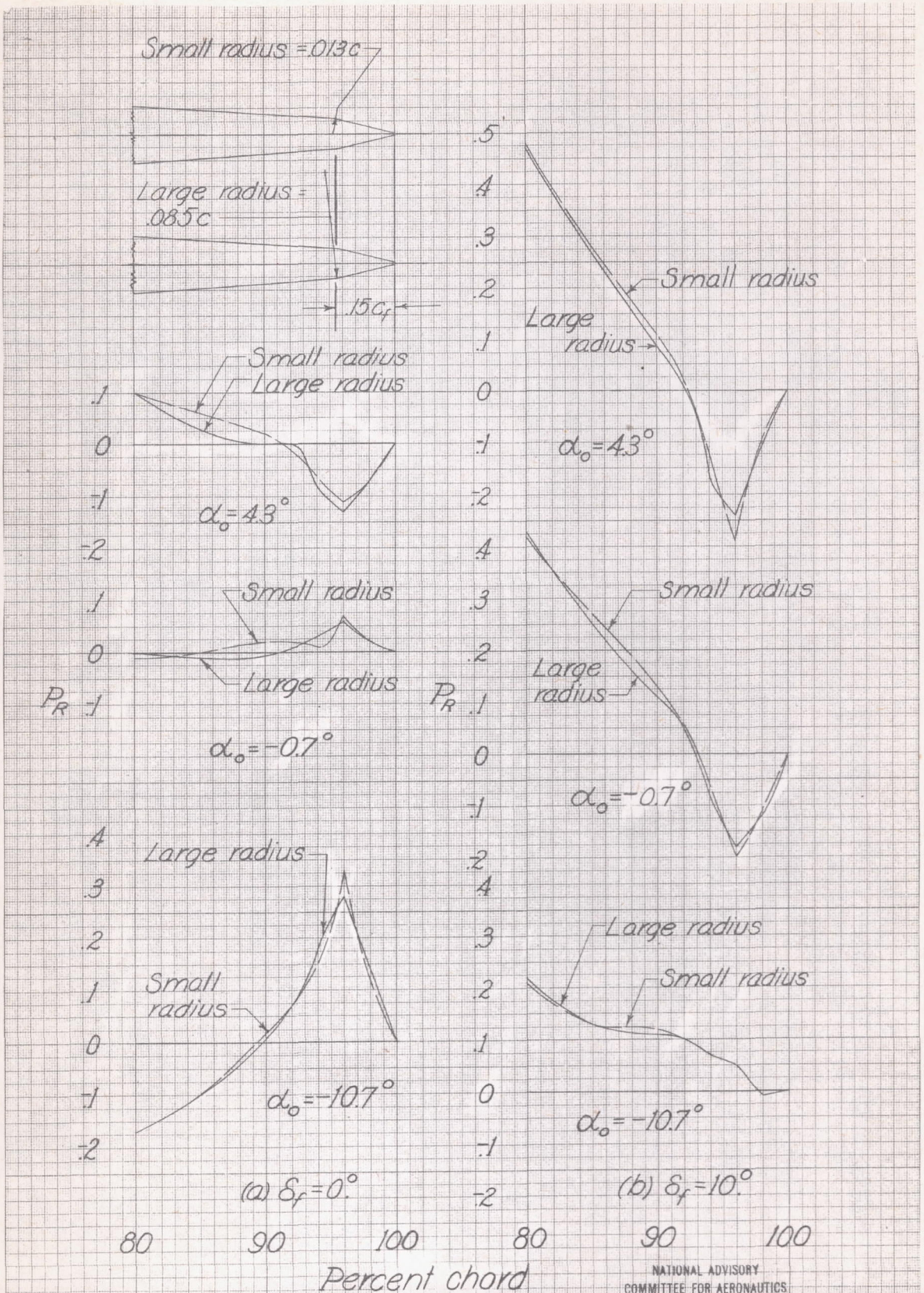

NATIONAL ADVISORY COMMITTEE FOR AERONAUTICS

Figure 11.-Comparison of resultant pressures over a 0.15c_f bevel with large and small radii. NACA 0009 airfoil; 0.30c flap; sealed gap.

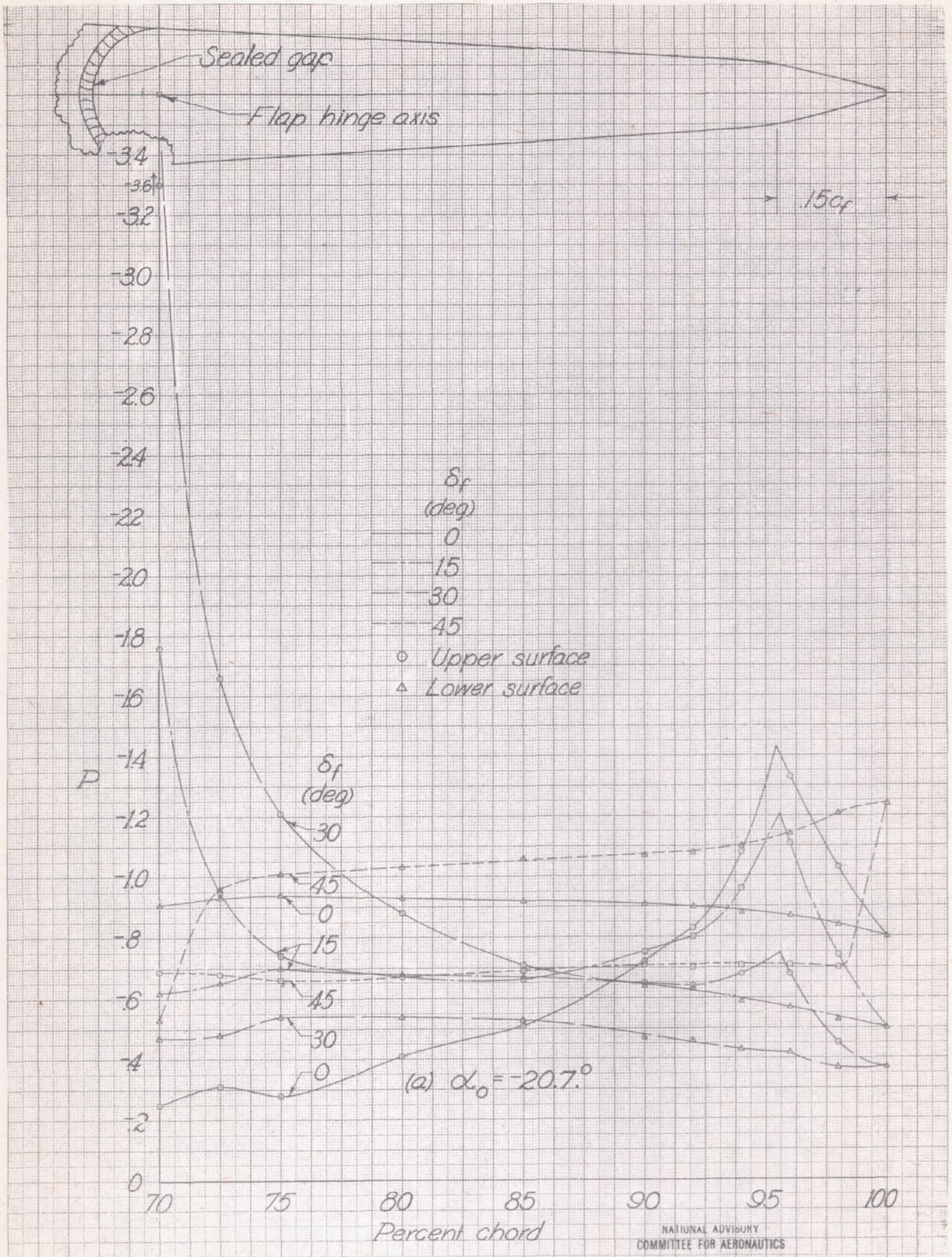

Figure 12.- Pressure distributions over a 0.30c flap having a $0.15c_f$ bevel at various angles of attack and flap deflections. NACA 0009 airfoil; sealed gap.

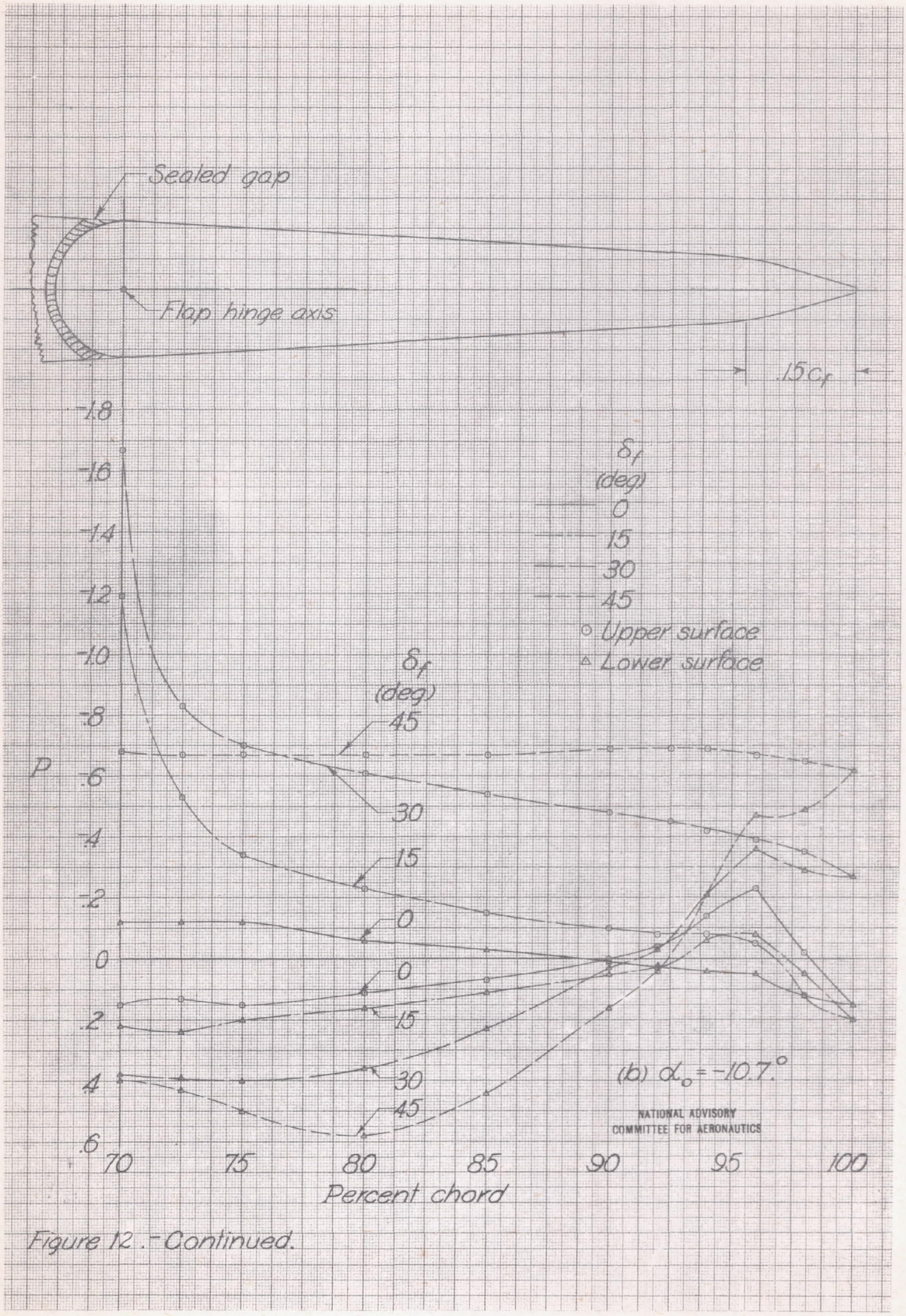

Figure 12.- Continued.

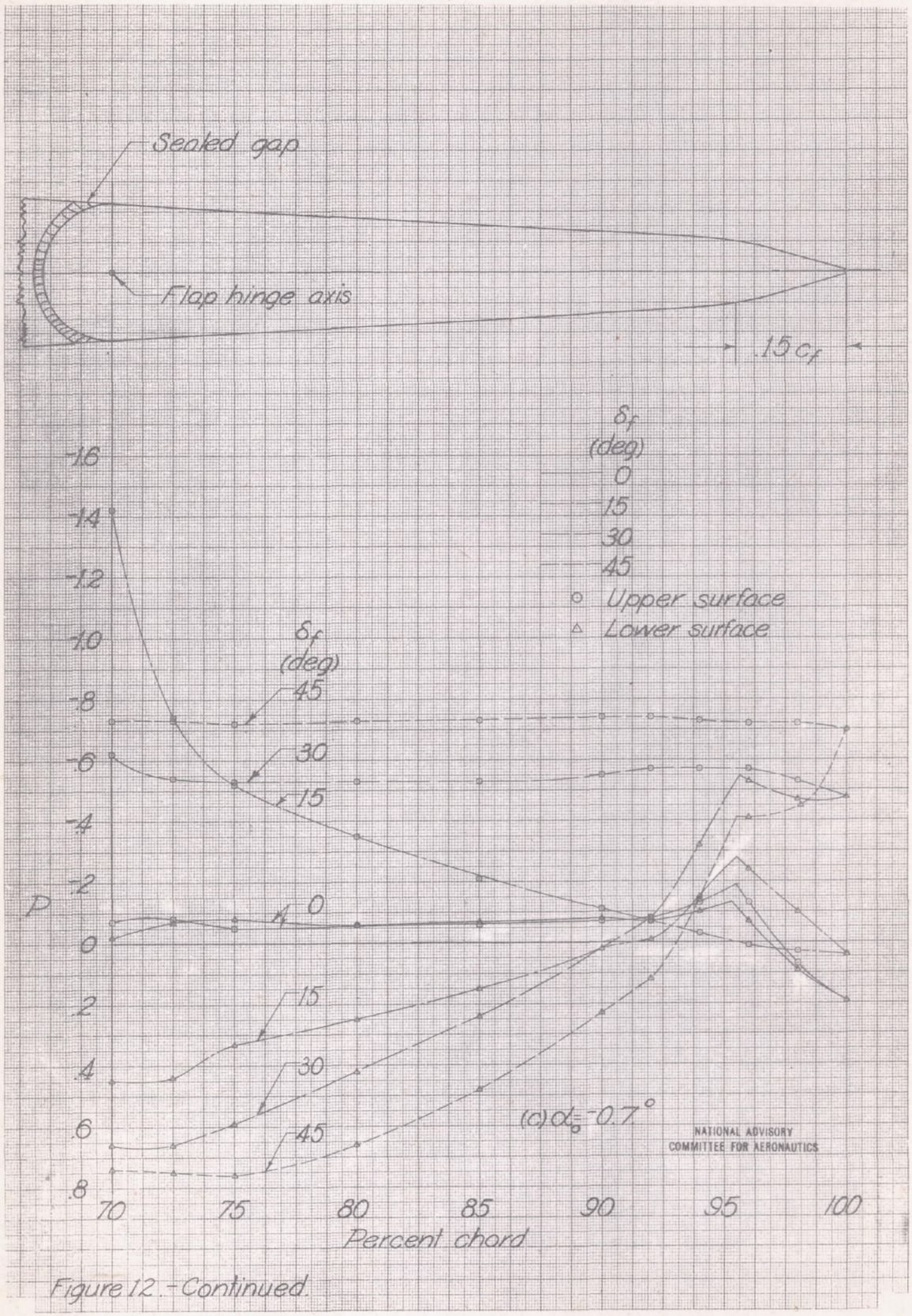

Figure 12.- Continued.

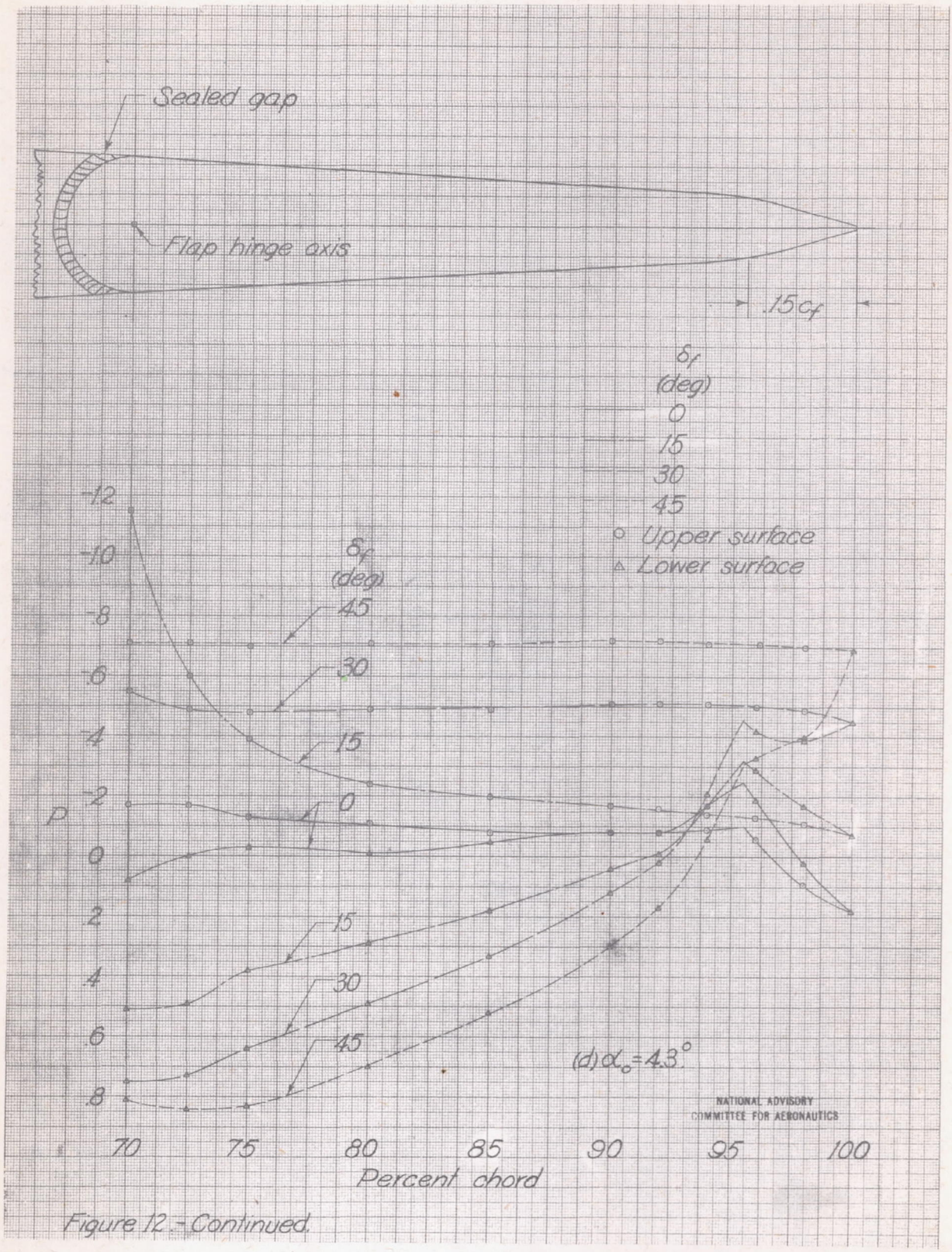

Figure 12.- Continued.

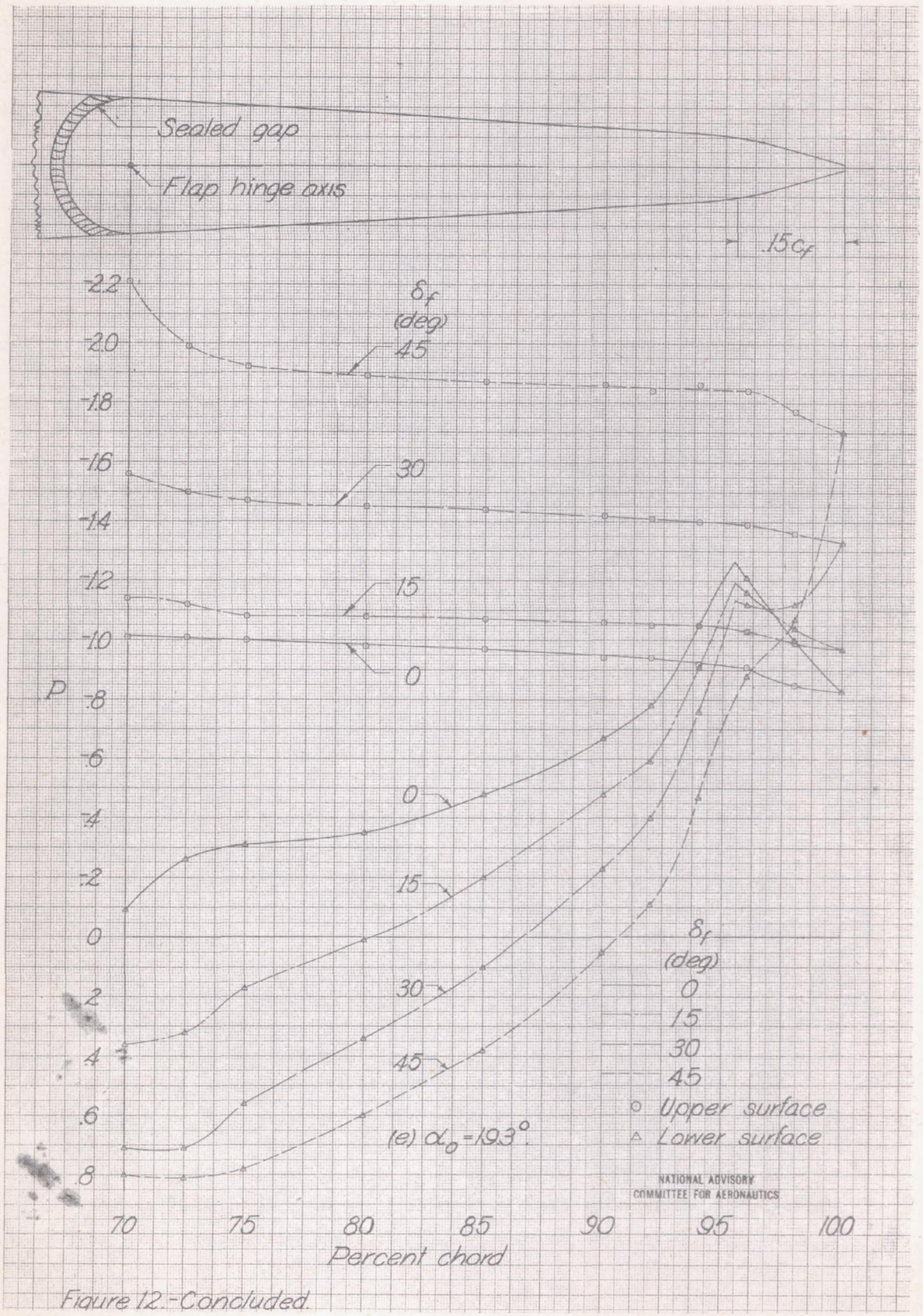

Figure 12.-Concluded.

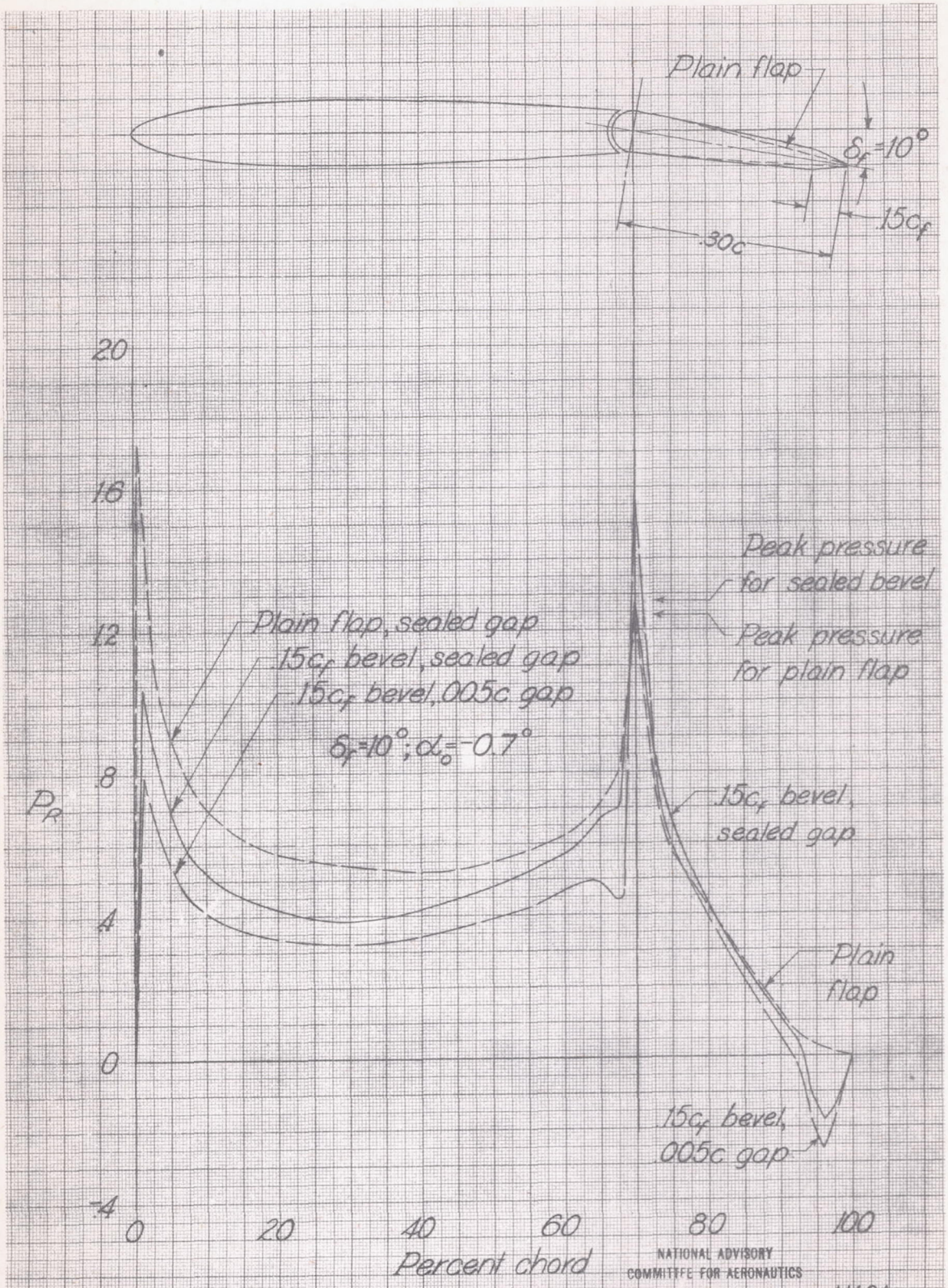

Figure 13.- Comparison of resultant pressures over an NACA 0009 airfoil having a 0.30c flap with and without a 0.15 c_f bevel. Plain-flap data from reference 5.

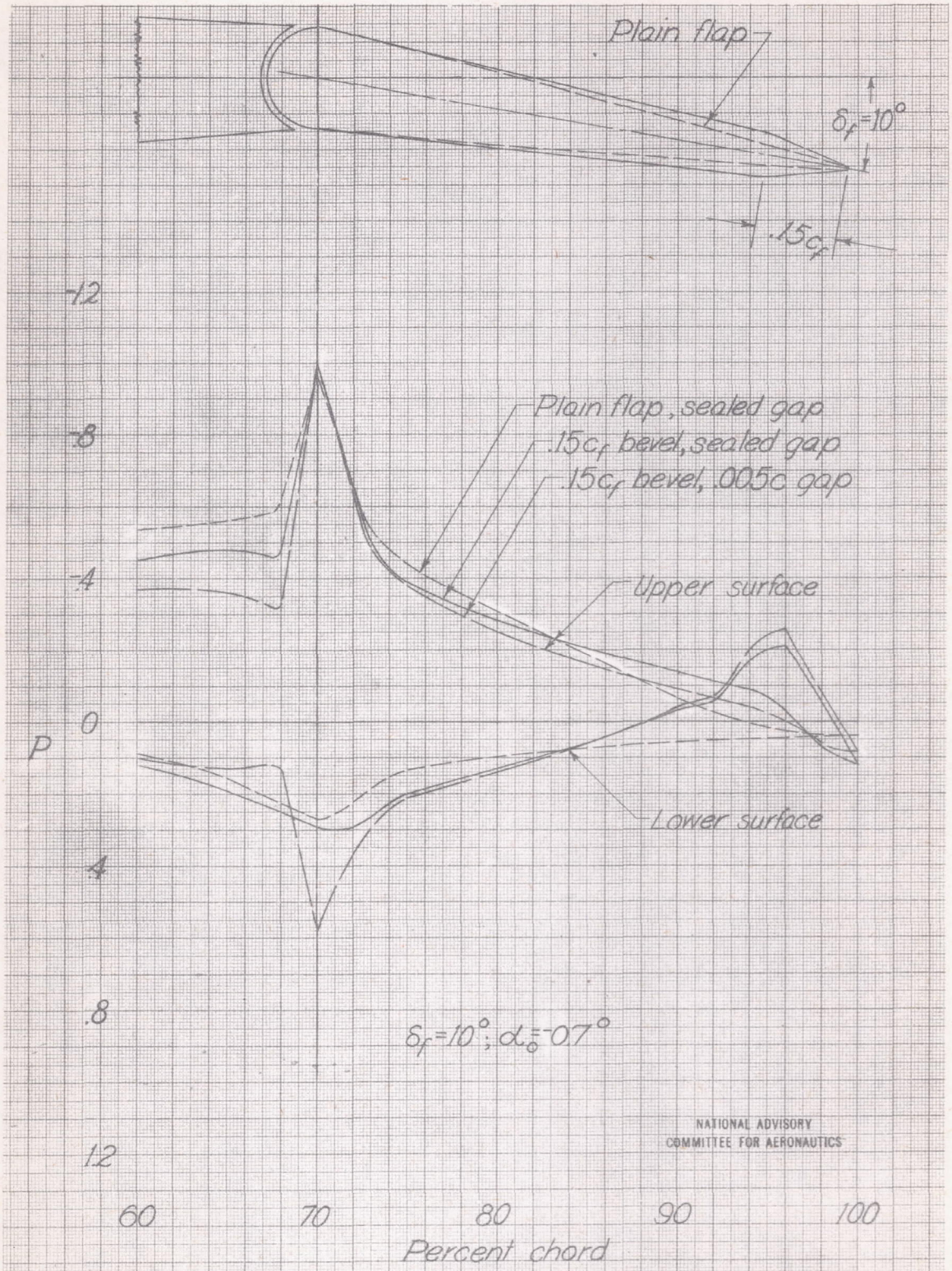

Figure 14.- Comparison of pressure distributions over rearward portion of an NACA 0009 airfoil having a 0.30c flap with and without a 0.15c_f bevel. Plain-flap data from reference 5.

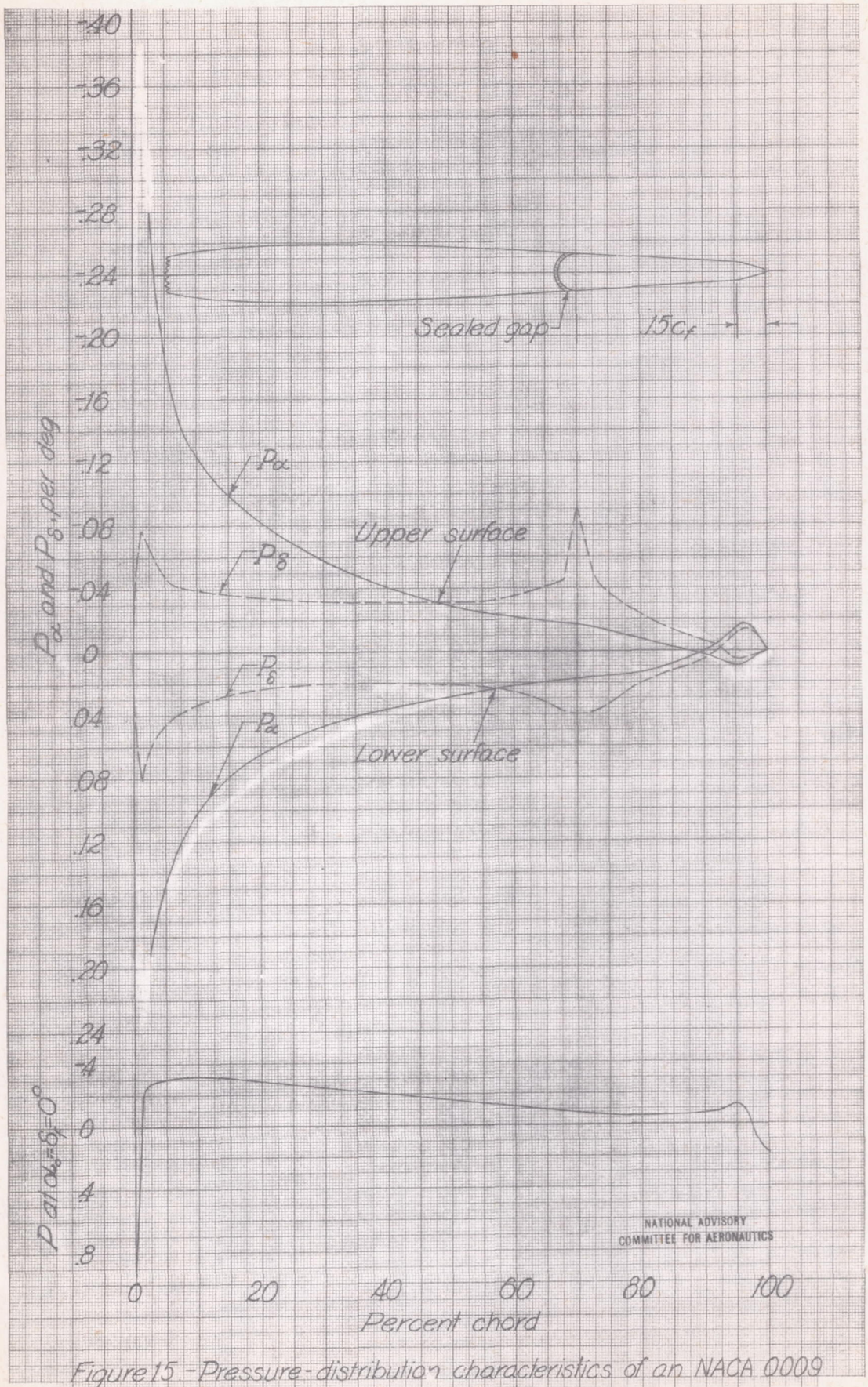

Figure 15.-Pressure-distribution characteristics of an NACA 0009 airfoil with a 0.30c flap having a 0.15c_f bevel. Sealed gap.

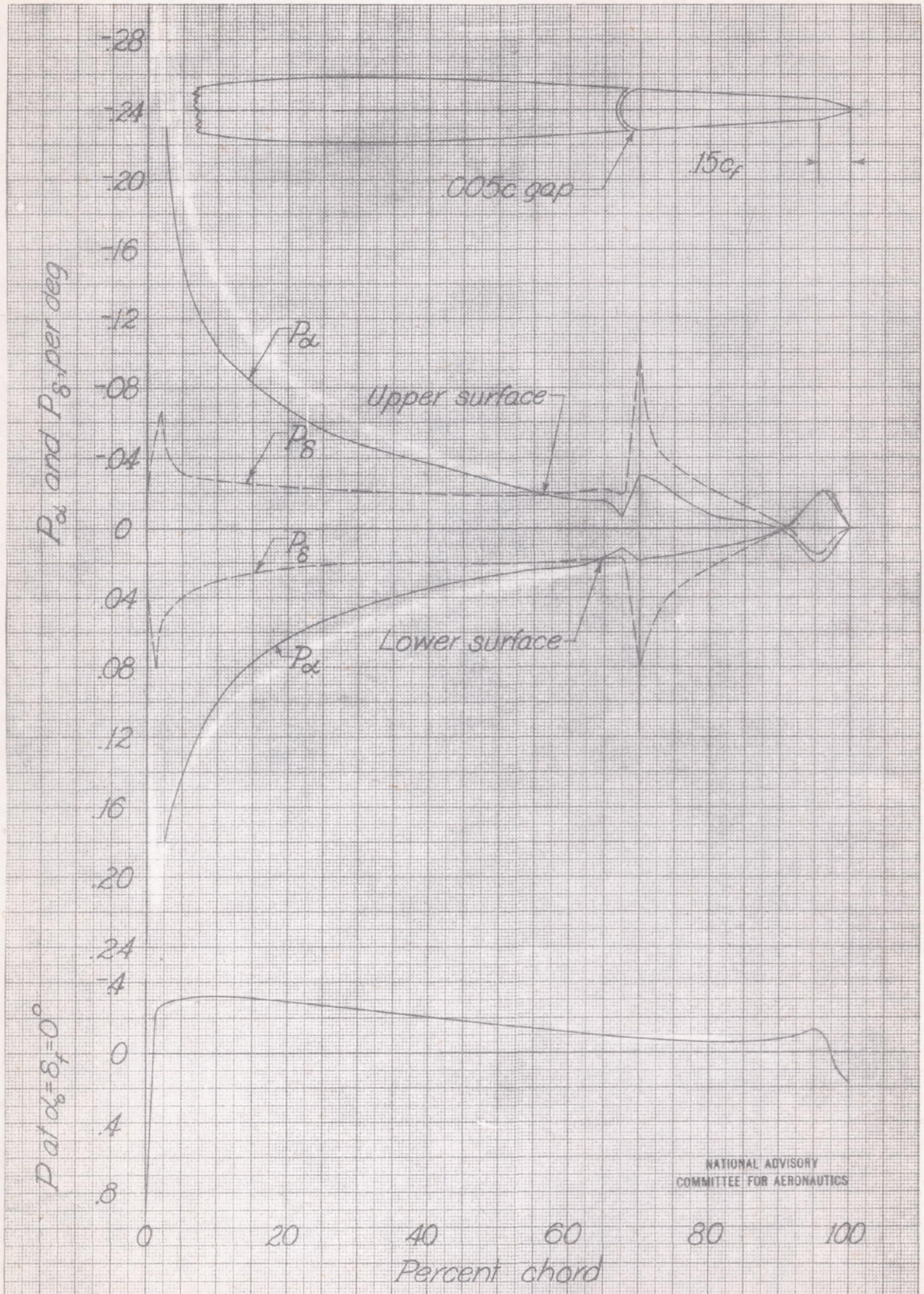

Figure 16.- Pressure-distribution characteristics of an NACA 0009 airfoil with a 0.30c flap having a $0.15c_f$ bevel, 0.005c gap.

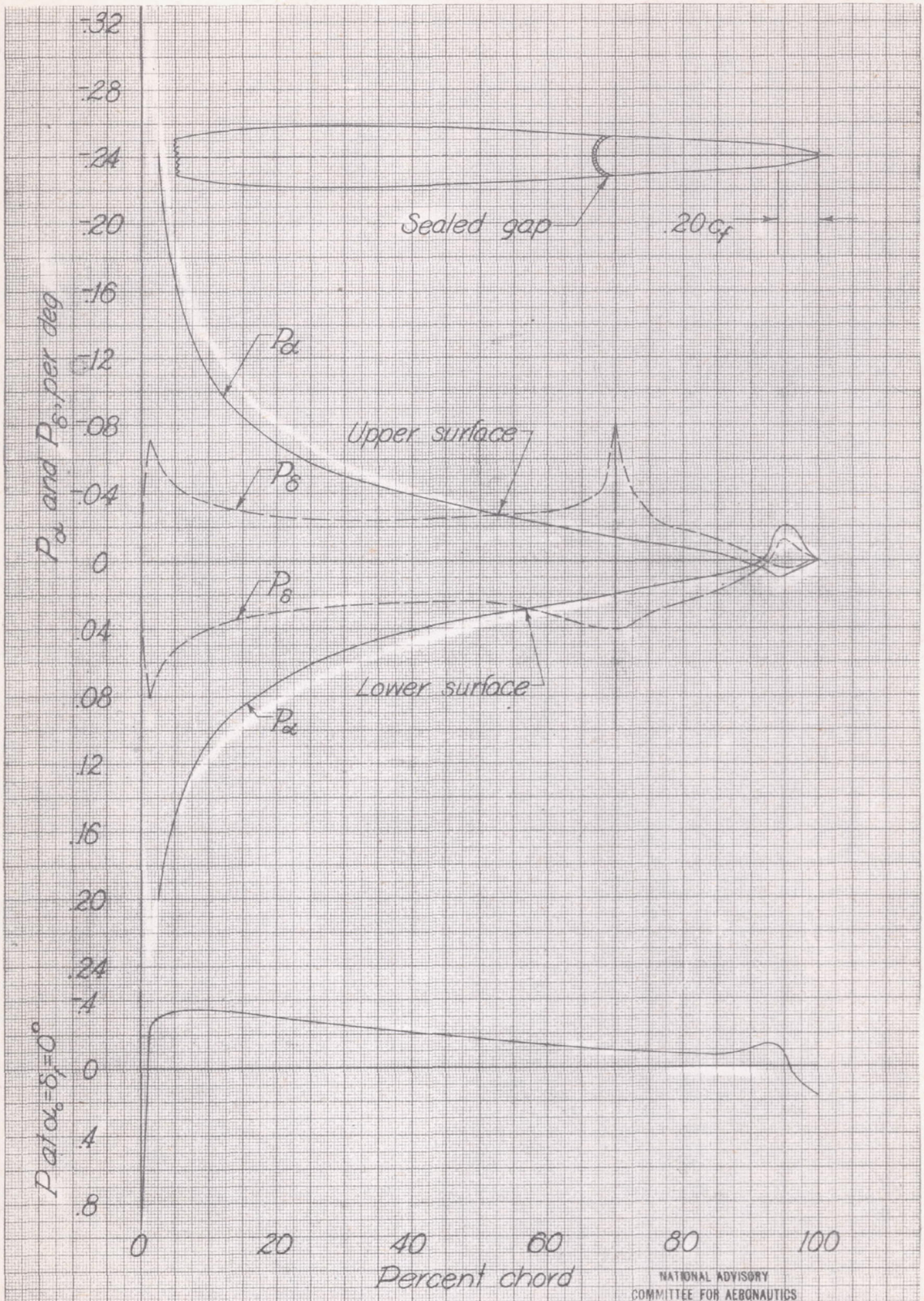

Figure 17.-Pressure-distribution characteristics of an NACA 0009 airfoil with a 0.30c flap having a $0.20c_f$ bevel. Sealed gap.

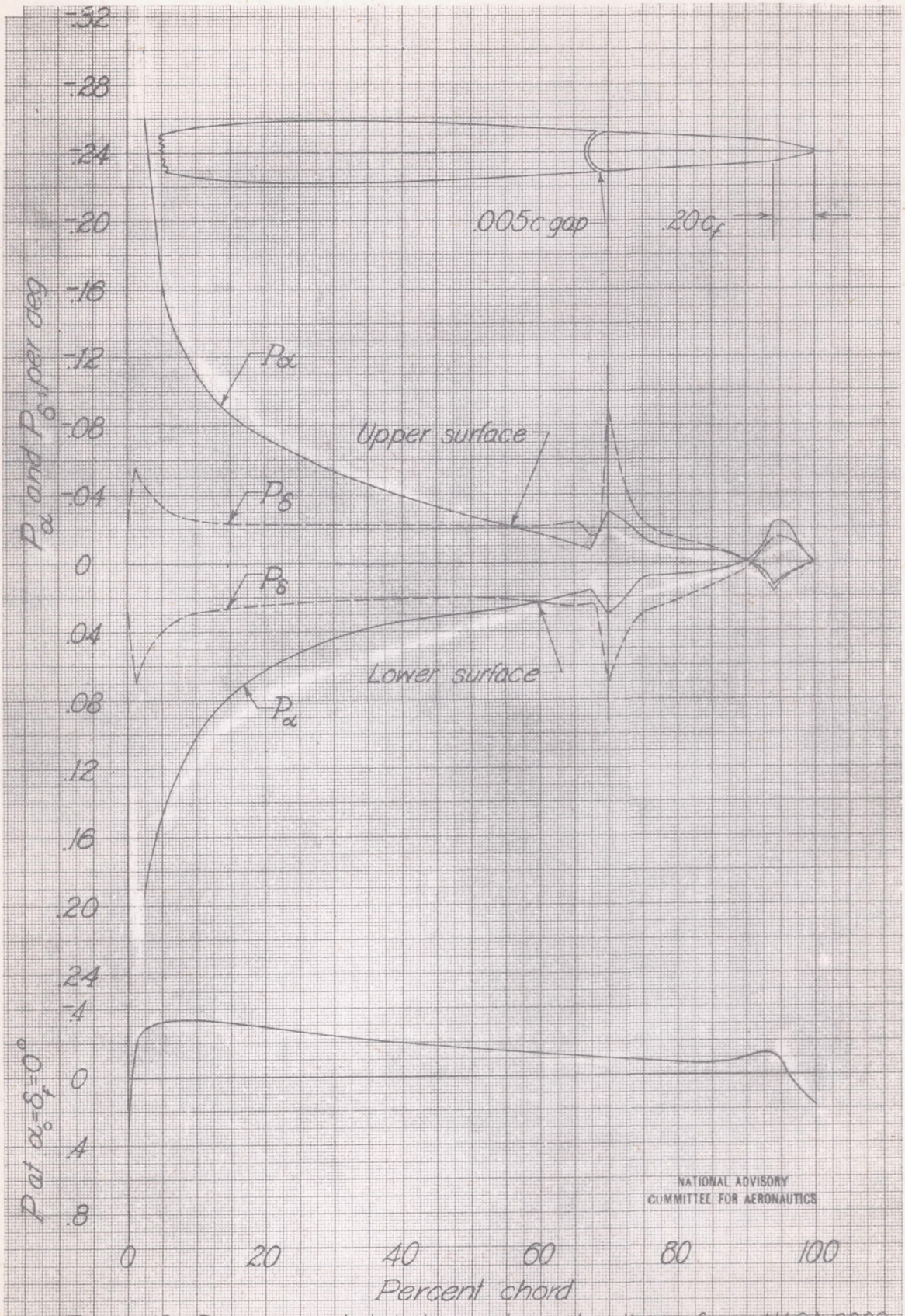

Figure 18.- Pressure-distribution characteristics of an NACA 0009 airfoil with a 0.30c flap having a $0.20c_f$ bevel. 0.005c gap.

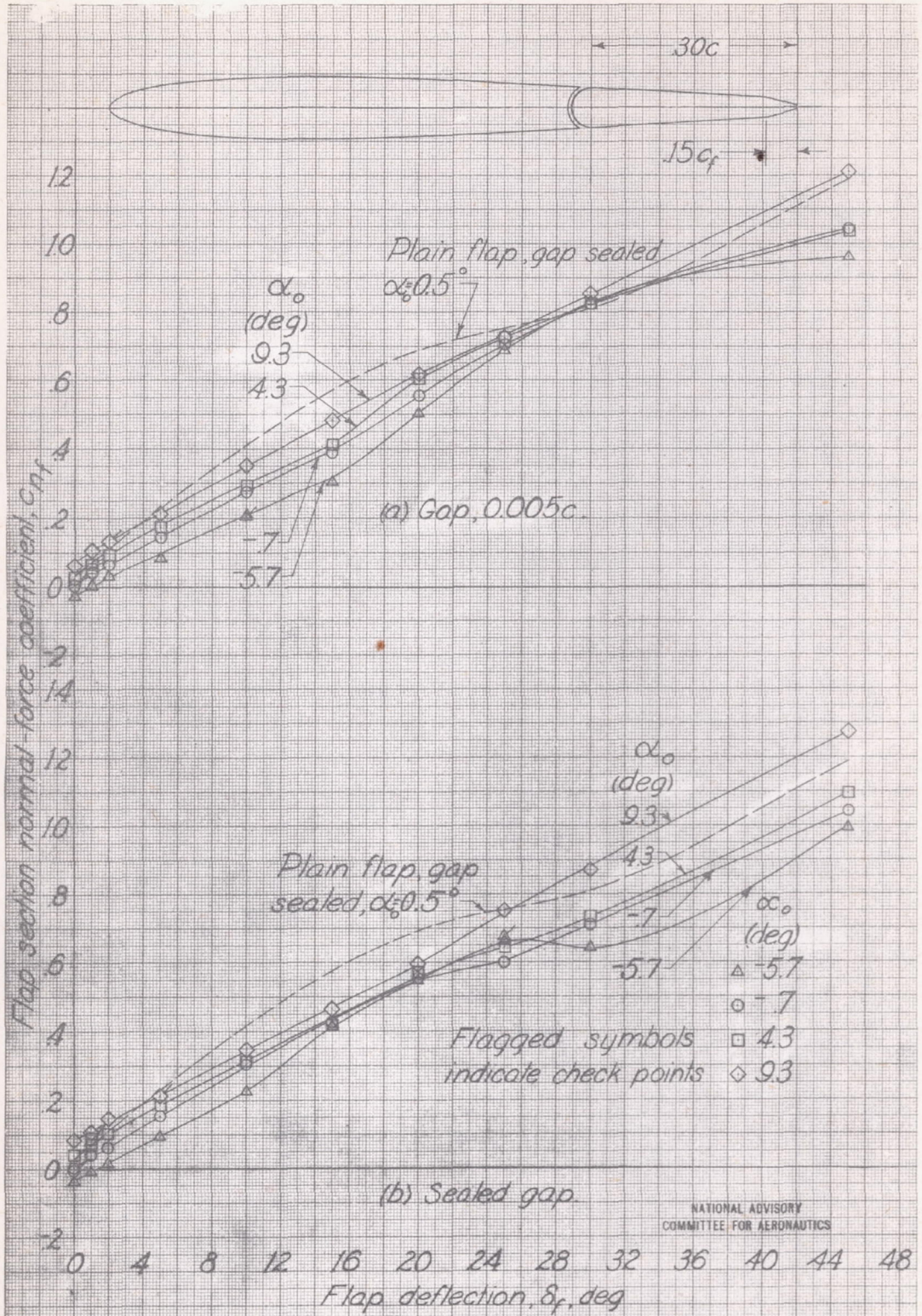

Figure 19.- Flap section normal-force coefficient as a function of the deflection of a 0.30c flap having a $0.15c_f$ bevel on an NACA 0009 airfoil. The included angle at the trailing edge is 30.4°. Plain-flap data from reference 5.

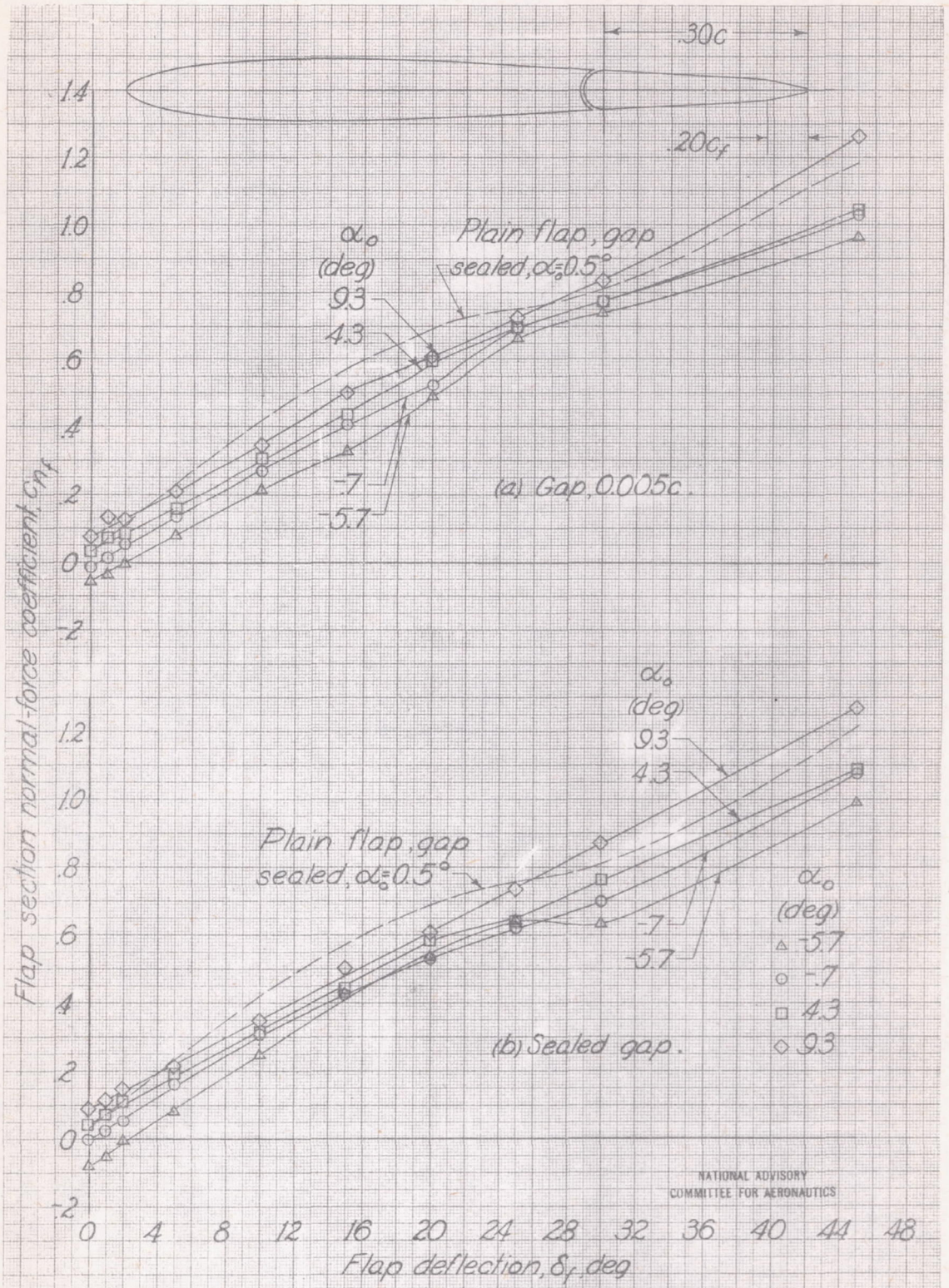

Figure 20.- Flap section normal-force coefficient as a function of the deflection of a 0.30c flap having a 0.20 c_f bevel on an NACA 0009 airfoil. The included angle at the trailing edge is 25.0°. Plain-flap data from reference 5.

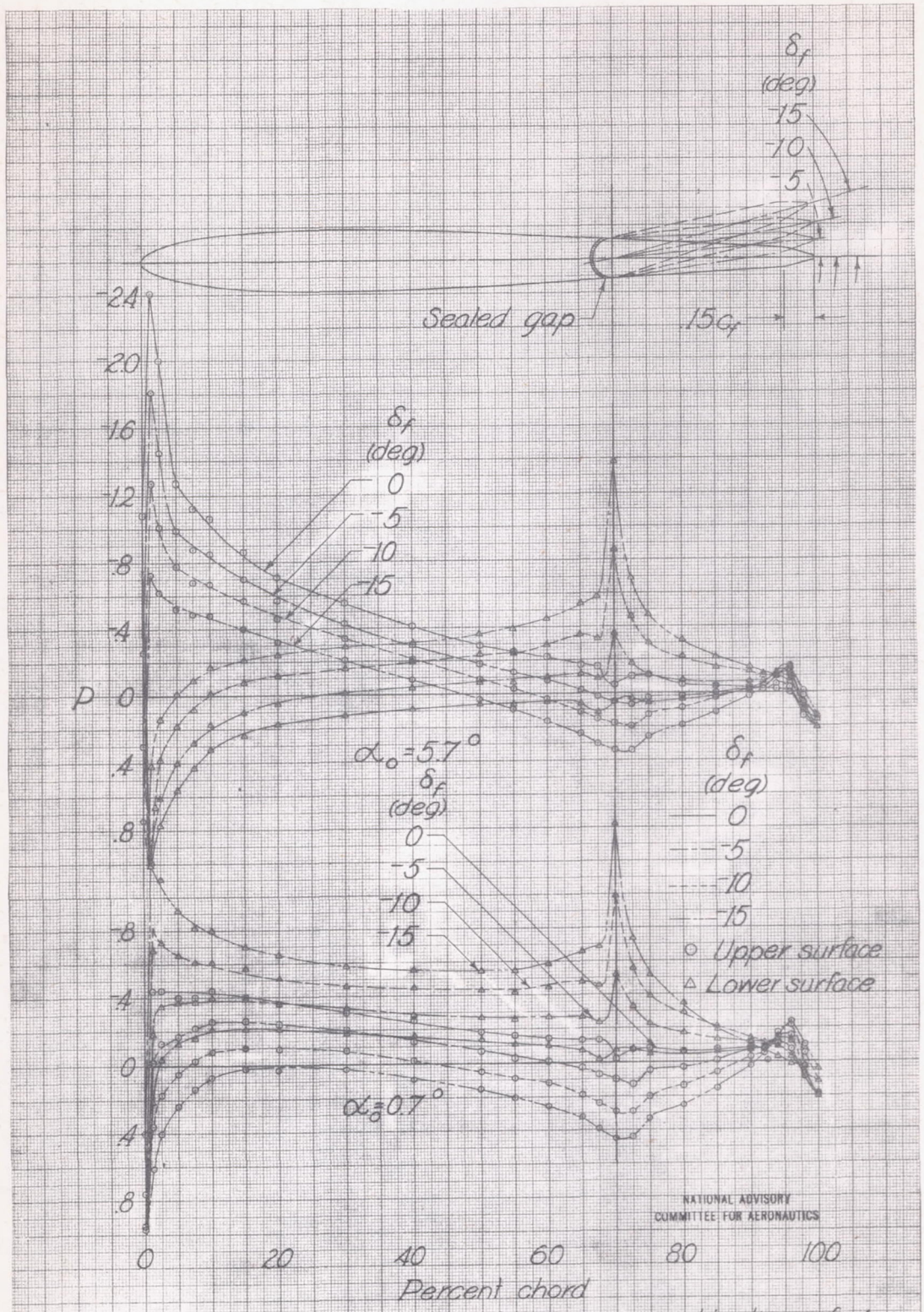

Figure 21.- Pressure distribution for various combinations of α_o and δ_f which might occur on horizontal tail of typical dive bomber in highly accelerated maneuvers at various speeds. NACA 0009 airfoil; 0.30c flap; sealed gap; $0.15c_f$ bevel.

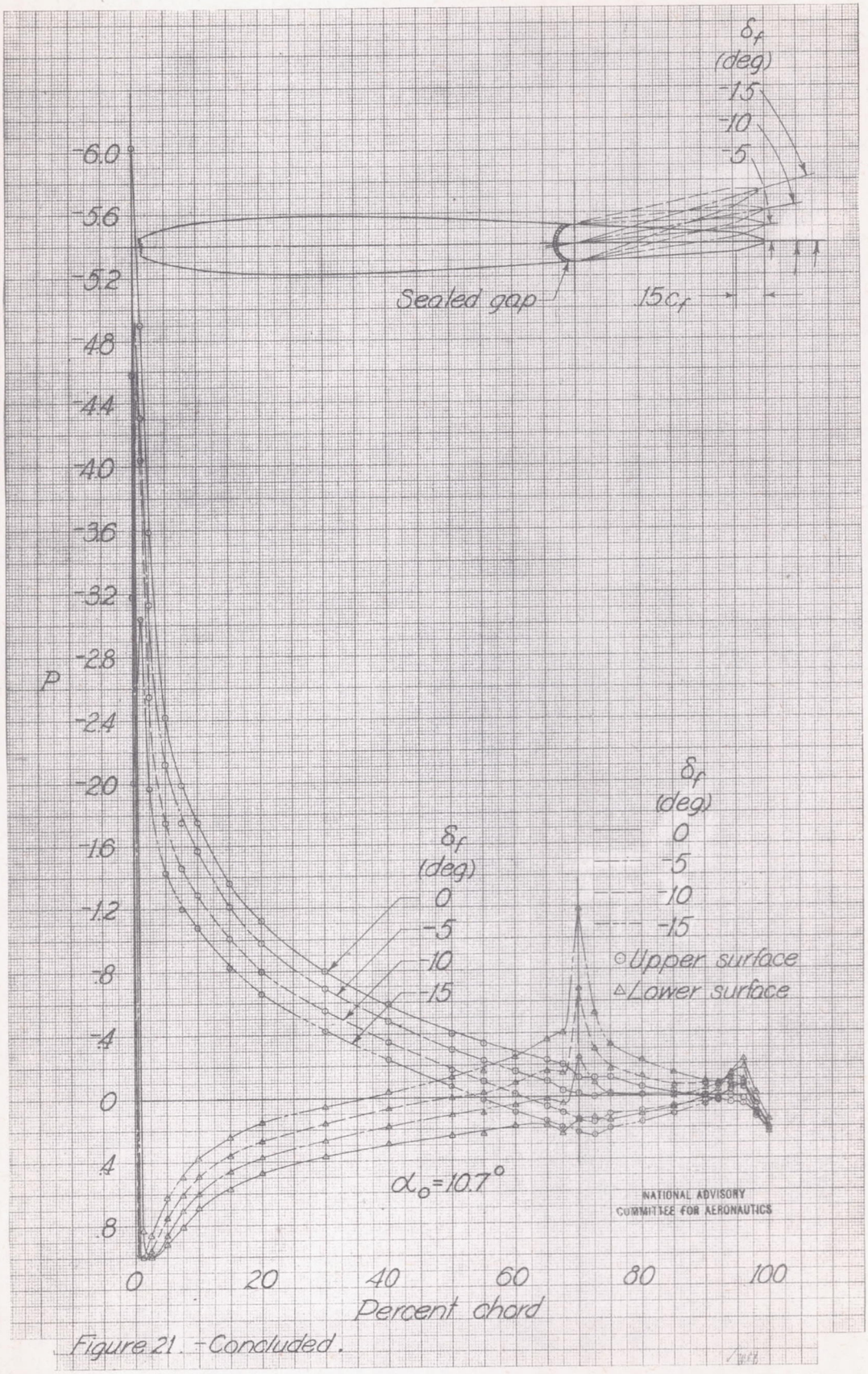

Figure 21.- Concluded.

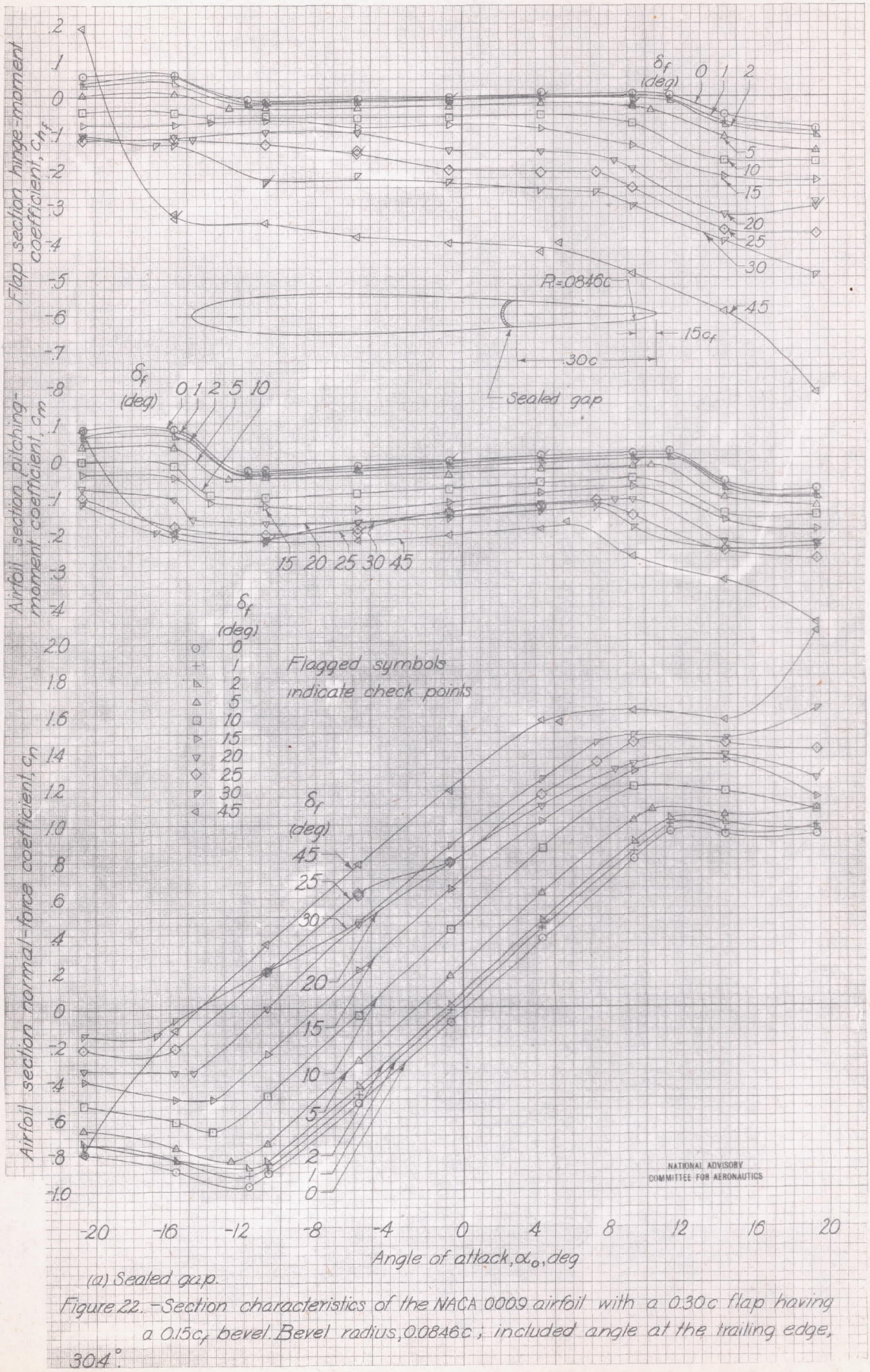

(a) Sealed gap.

Figure 22.- Section characteristics of the NACA 0009 airfoil with a 0.30c flap having a 0.15c_f bevel. Bevel radius, 0.0846c; included angle at the trailing edge, 30.4°.

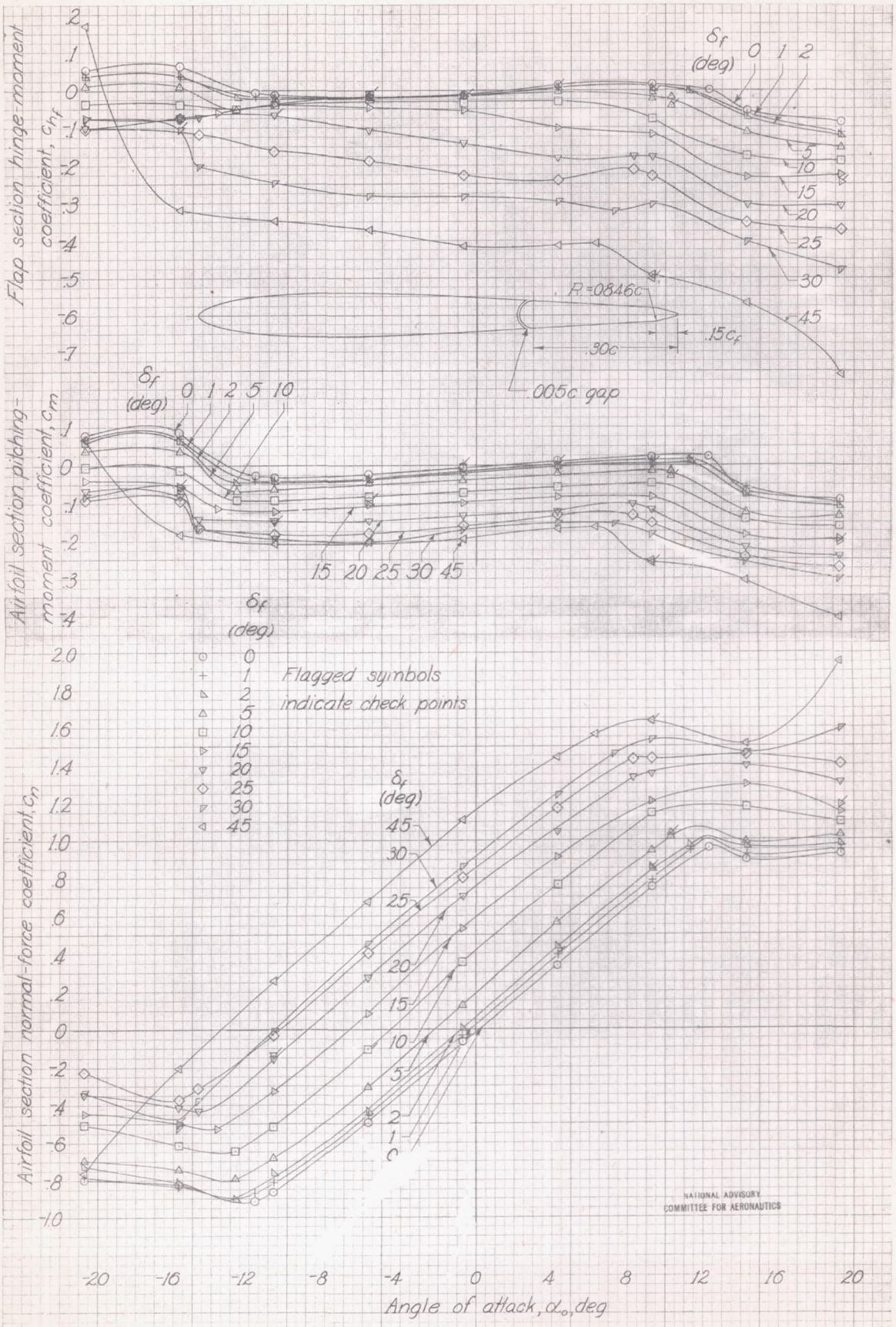

(b) Gap, 0.005c.

Figure 22.-Concluded.

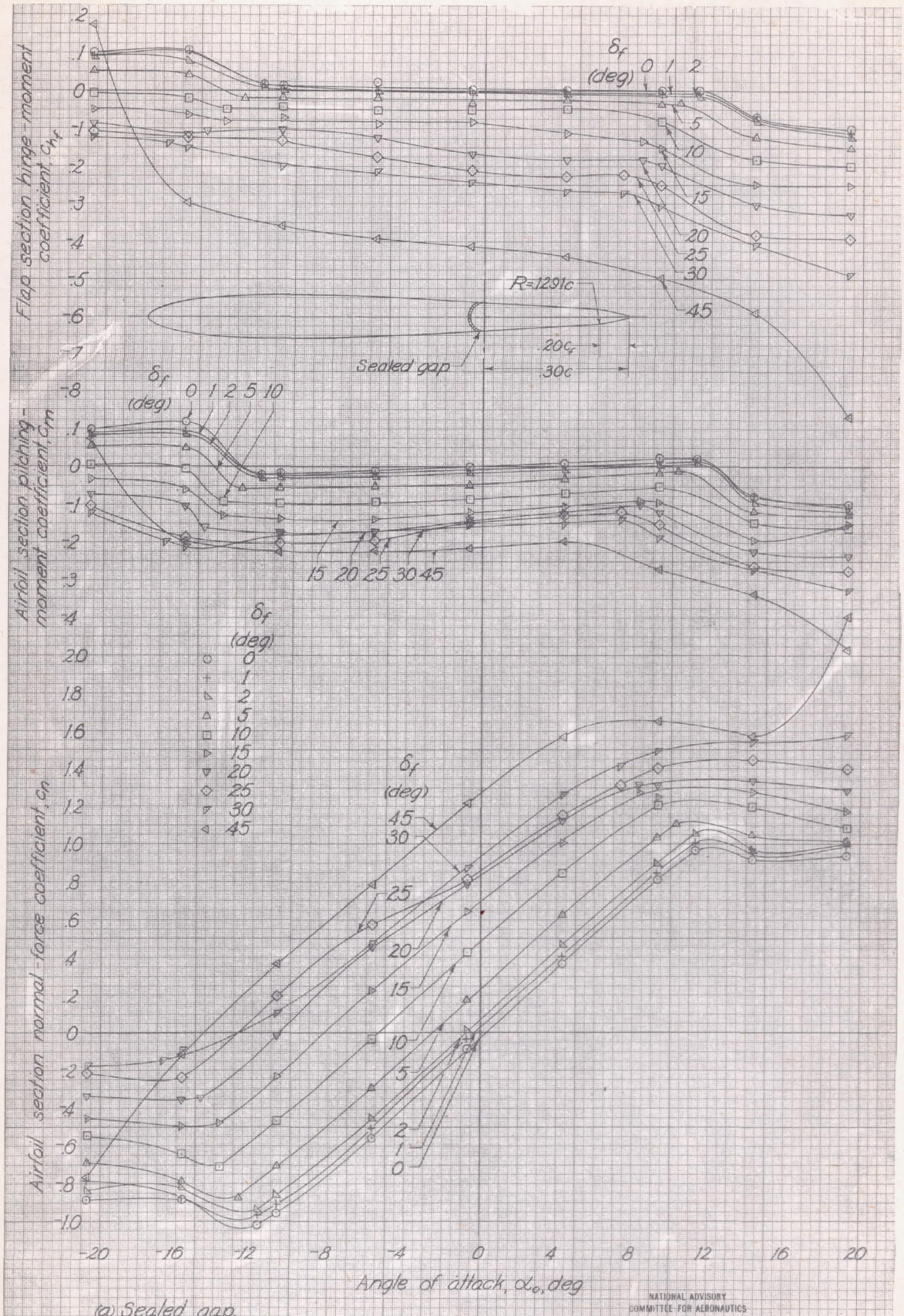

(a) Sealed gap.

Figure 23.- Section characteristics of the NACA 0009 airfoil with a 0.30c flap having a 0.20c_f bevel. Bevel radius, 0.1291c; included angle at trailing edge, 25.0°.

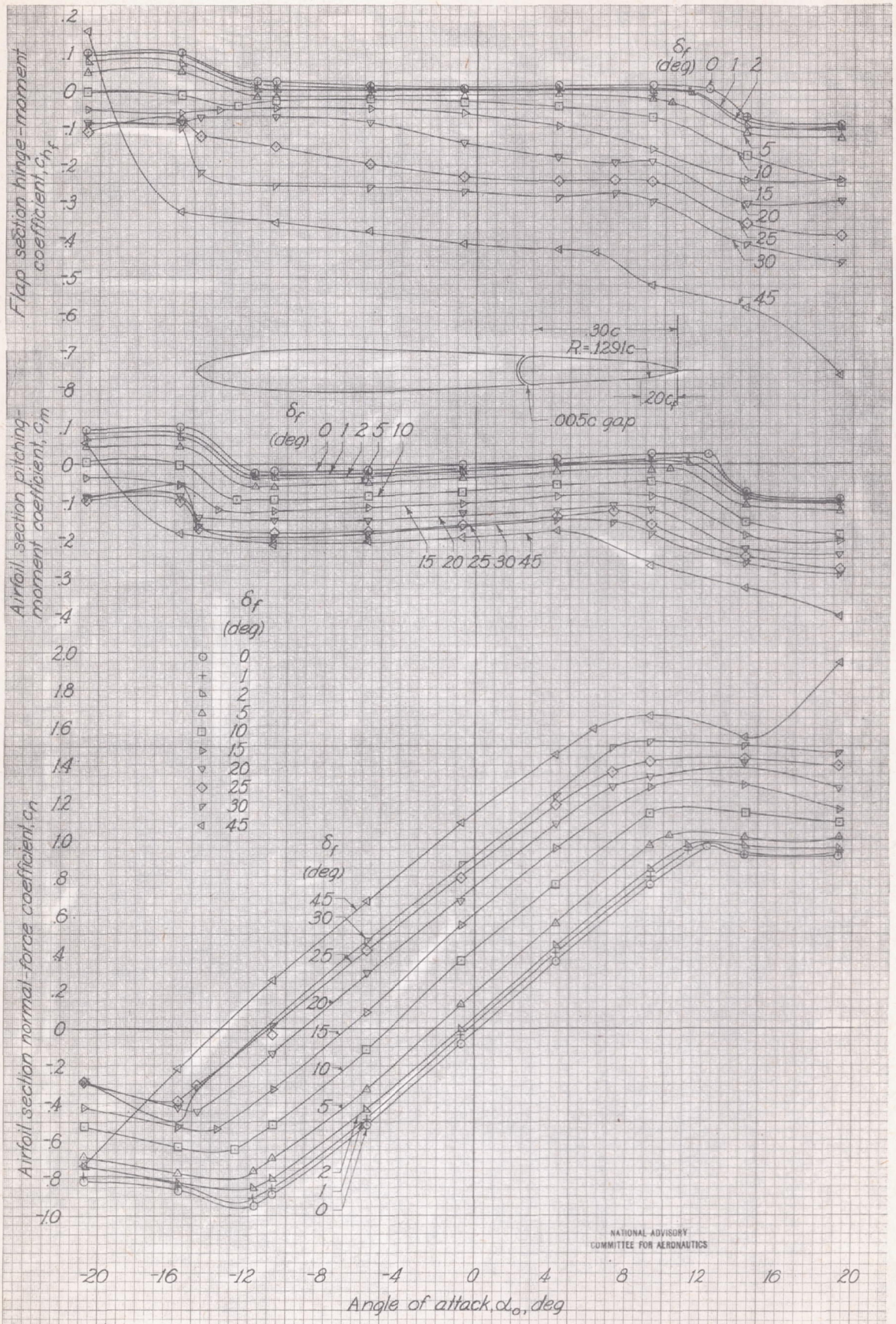

(b) Gap, 0.005c.

Figure 23.- Concluded.

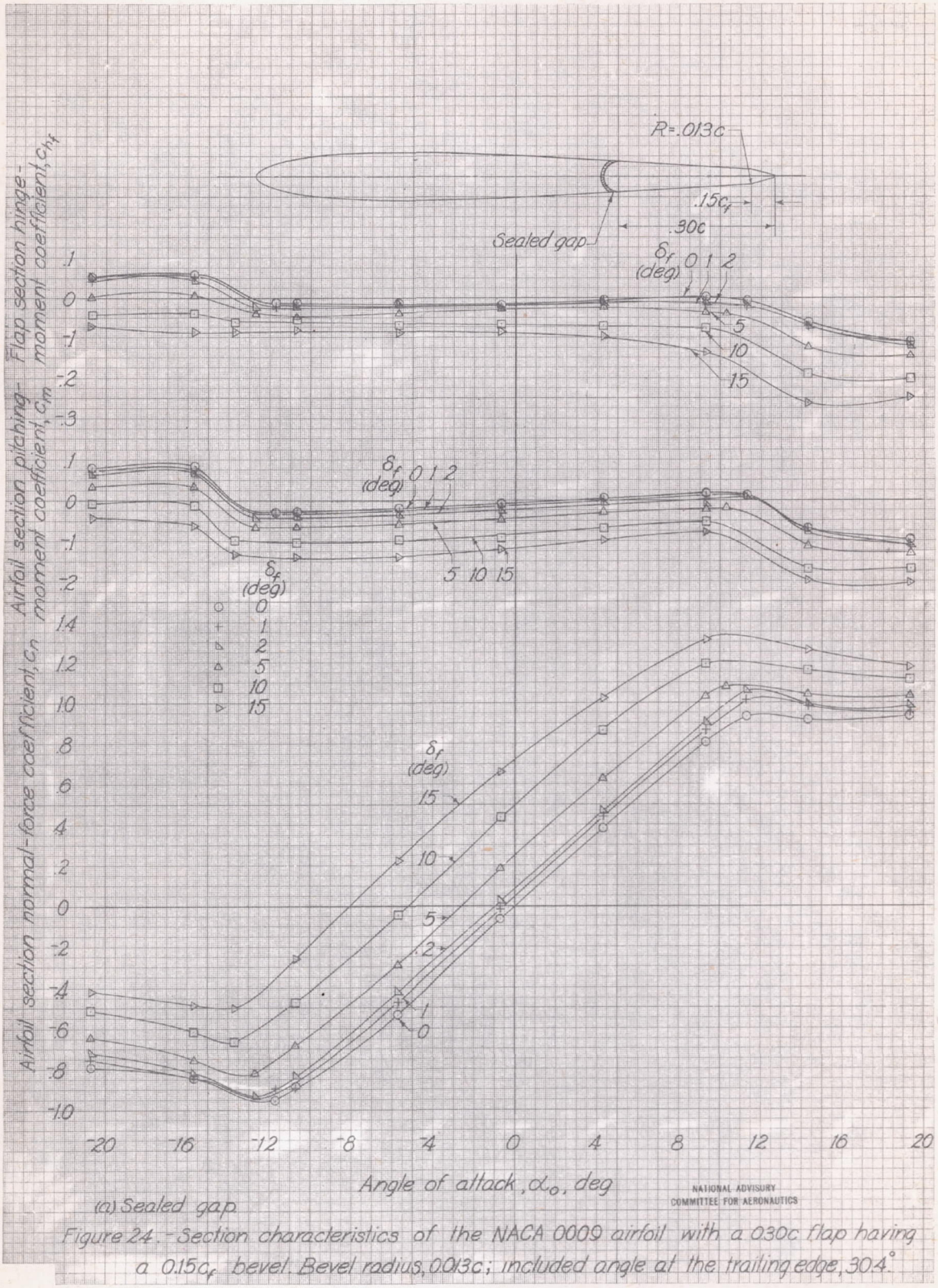

(a) Sealed gap.

Figure 24.- Section characteristics of the NACA 0009 airfoil with a 0.30c flap having a 0.15c_f bevel. Bevel radius, 0.013c; included angle at the trailing edge, 30.4°.

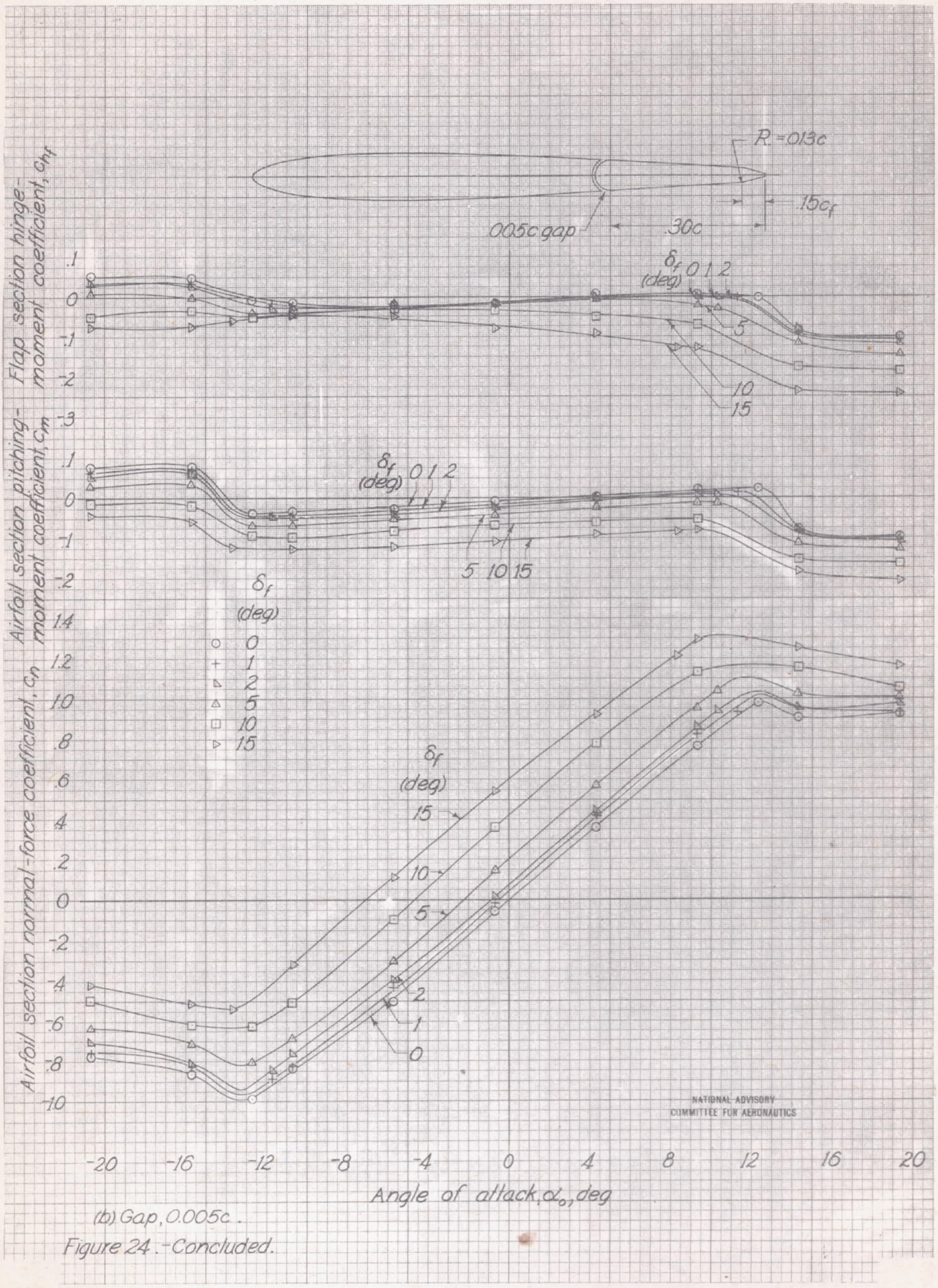

(b) Gap, 0.005c.

Figure 24.- Concluded.

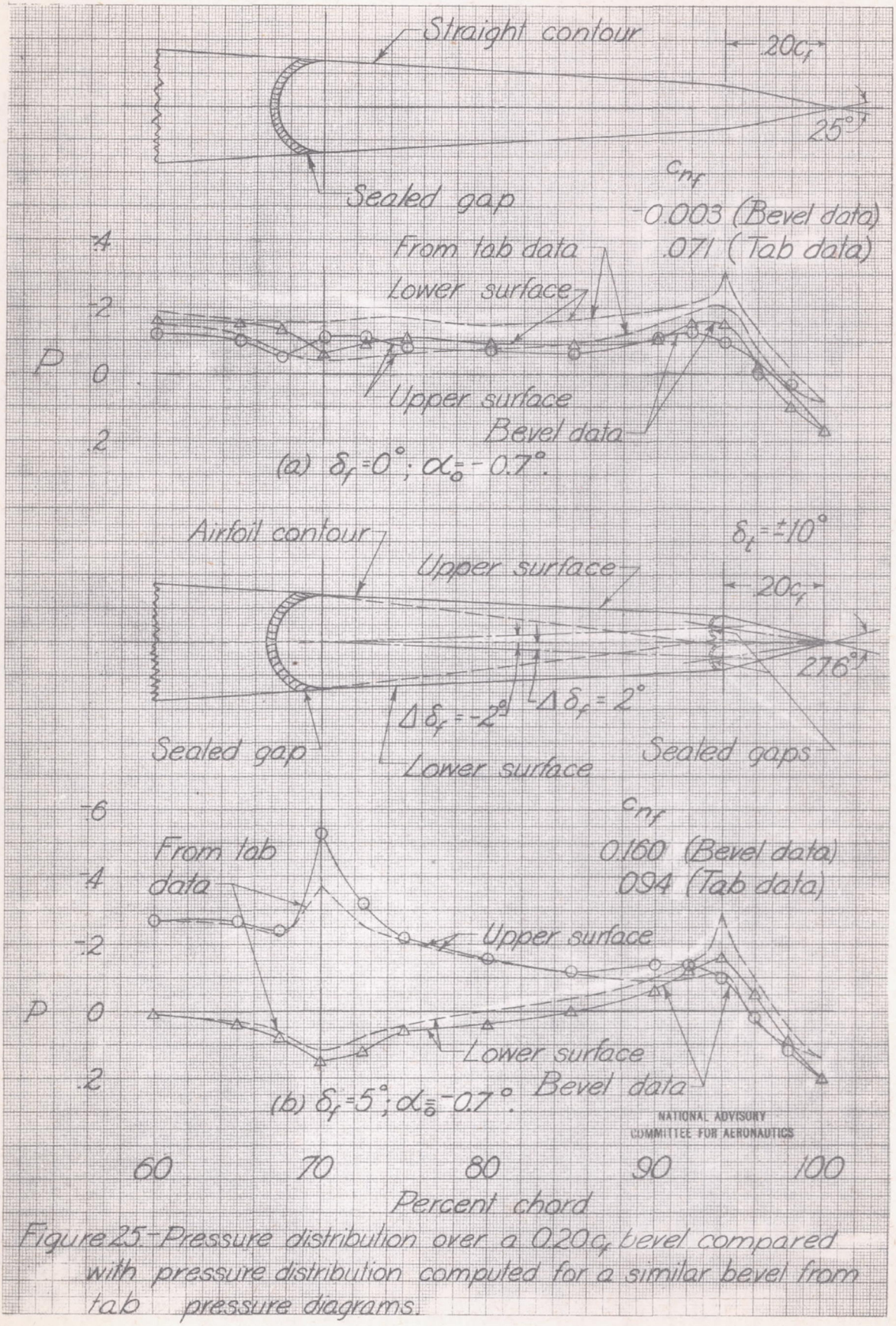

Figure 25.- Pressure distribution over a $0.20c_f$ bevel compared with pressure distribution computed for a similar bevel from tab pressure diagrams.

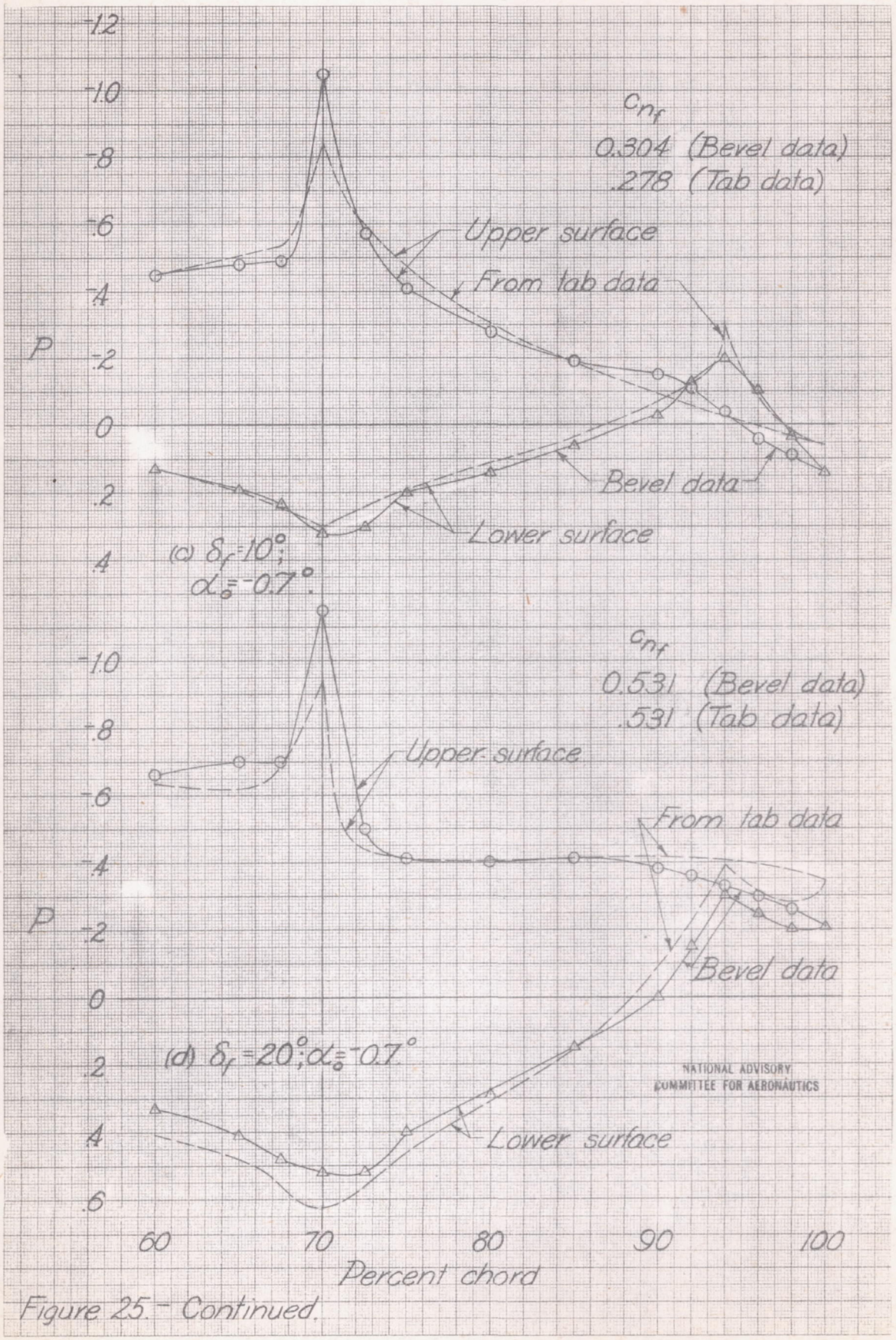

Figure 25.- Continued.

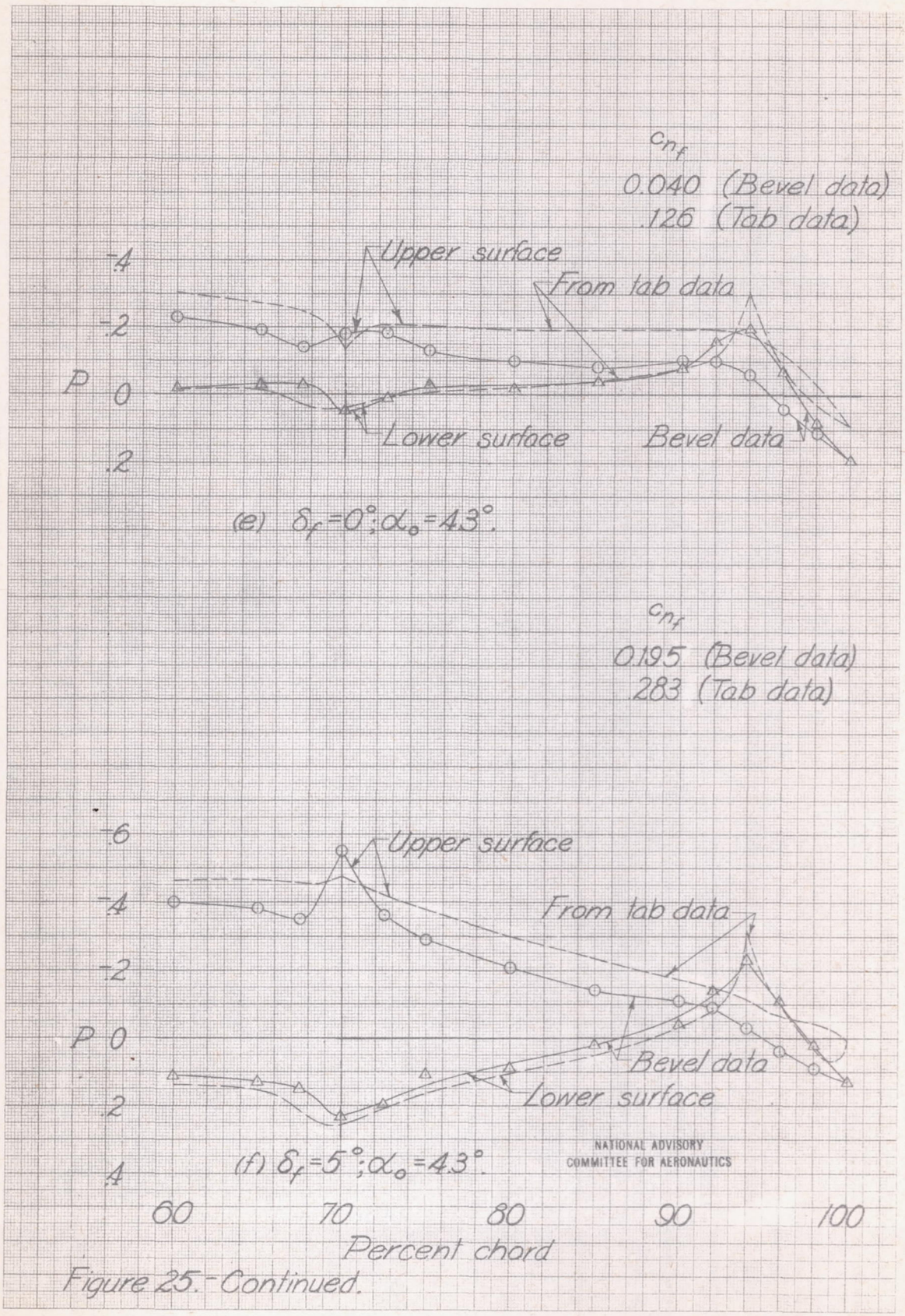

Figure 25.- Continued.

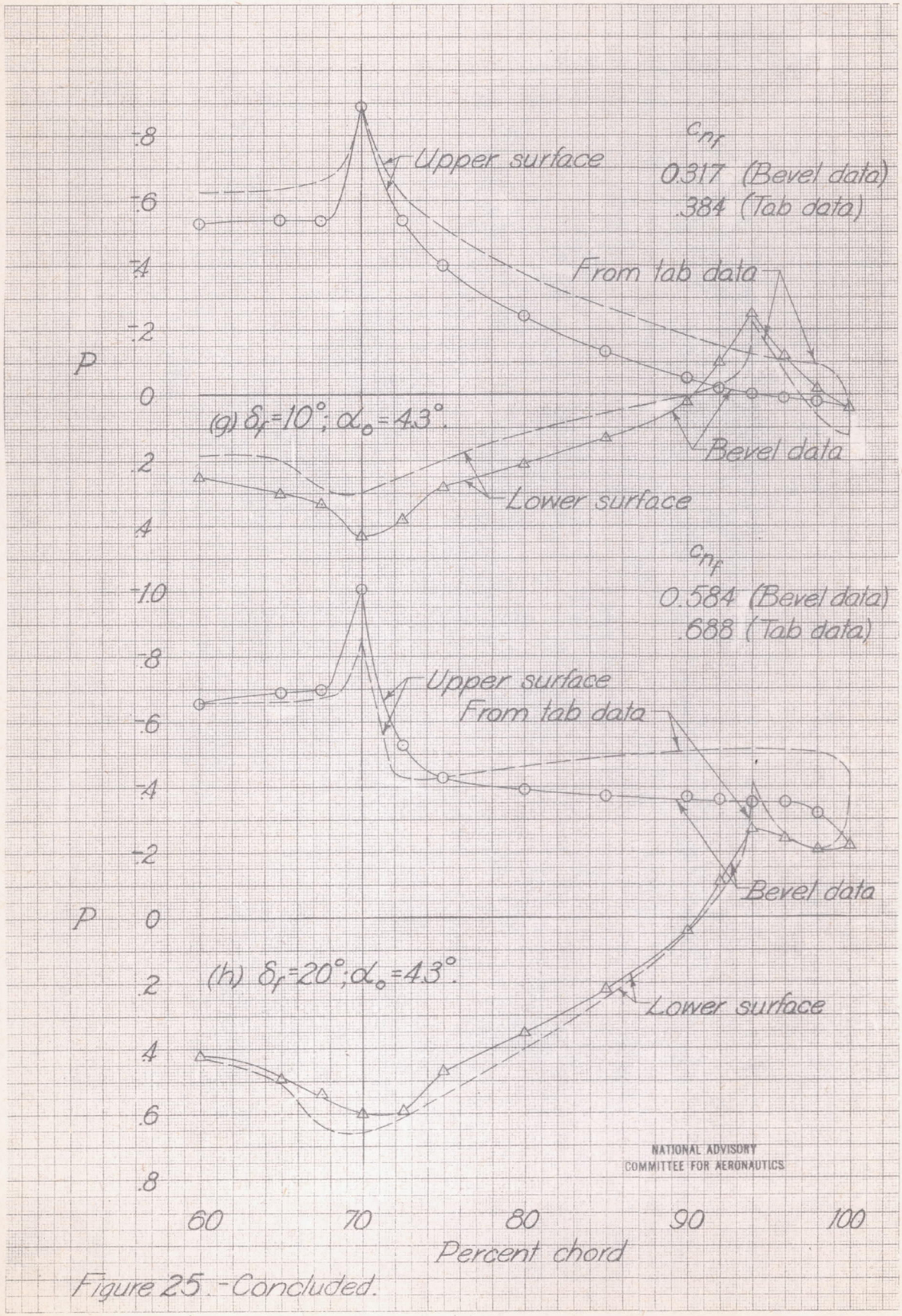

Figure 25. - Concluded.